Applied Catalysis B: Environmental 305 (2022) 121052

Contents lists available at ScienceDirect

Applied Catalysis B: Environmental

journal homepage: www.elsevier.com/locate/apcatb

Kinetics of fatty acid ketonization in liquid phase with anatase and rutile TiO_2 catalysts

Bert Boekaerts, Ward Lorenz, Joost Van Aelst, Bert F. Sels *

Department of Microbial and Molecular Systems (M^2S), Center for Sustainable Catalysis and Engineering (CSCE), KU Leuven, Celestijnenlaan 200F, 3001 Leuven, Belgium

ARTICLE INFO

Keywords:
Ketonization
Fatty acid
TiO_2 catalyst
Kinetic study
Liquid phase

ABSTRACT

Catalytic ketonization of carboxylic acids is promising for the synthesis of renewable products. Despite its potential, fatty acid ketonization and its kinetics in the liquid phase are less investigated. This work encompasses kinetic evaluation of two TiO_2 catalysts (anatase and rutile) for C-C coupling of C_{12}-C_{18} fatty acids in inert dodecane solvent. The rutile catalyst, with higher Lewis acid density, showed higher intrinsic activity and more favorable activation energy barriers. Unfortunately, this material suffers from stronger product inhibition by ketone, water and carbon dioxide compared to anatase. Langmuir-Hinshelwood kinetic models were developed and validated against the experimental data, supporting that C-C coupling of adsorbed species is rate determining in the ketonization mechanism. The Lewis acid site density and distance between active Ti species at the surface were invoked to explain the activity patterns. The impacts of substrate chain length, solvent and liquid phase purging on the ketonization kinetics were investigated, showcasing potential for future improvements.

1. Introduction

Ketonization of carboxylic acids is a unique C-C coupling reaction that converts two carboxylic acid molecules into an internal ketone with increased chain length, and water and carbon dioxide side products [1]. Via this chemical pathway, carboxylic acids present in lignocellulose and oleochemical biomass can be valorized into renewable fuels and chemicals (or their intermediates) [2]. Indeed, pyrolysis bio-oil and its model compounds, typically C_2-C_4 carboxylic acids, have been studied extensively as substrates for this C-C coupling reaction [3–5]. In contrast, ketonization studies utilizing vegetable oils and animal fats (C_{12}-C_{18} fatty acids) are far less prevalent in literature, even though their specific chain length, limited chemical functionality and large scale availability should make them attractive substrates to synthesize renewable C_{23}-C_{35} ketone bio-waxes [6]. Besides direct use as (wax type) end products [7], consecutive hydrodeoxygenation and hydro-isomerisation of these bio-based compounds yields hydrocarbon wax and lubricant products [8].

Ketonization of carboxylic acids has been the subject of critical review [2,9–11]. From the large array of (heterogeneous) catalysts employed, metal oxides, and in particular amphoteric TiO_2, CeO_2, ZrO_2, are presented as most suitable due to a combination of high activity, selectivity (and stability) for this reaction. Latest literature indicates that their active surface sites, coordinatively unsaturated Lewis acid-base M^{x+}-O^{y-} pairs, catalyze the ketonization reaction via a β-ketoacid mechanism [12–16]. Several reports have been published on the kinetics of catalytic ketonization, almost exclusively when starting from C_2-C_4 acids in gas phase processes.

For instance, the C-C coupling of acetic acid with a bifunctional Ru/TiO_2 catalyst has been described by a power law equation, revealing a positive observed substrate reaction order value of 1.6 [17]. Multiple groups have reported an asymptotic relationship between the reaction rate and initial carboxylic acid concentration, resulting in fractional observed substrate orders, signaling the transition from a second [18] or first [19] to zero order reaction and saturation of the catalytic sites on the surface [20,21]. Oppositely, negative partial orders were found for all three reaction products, i.e. for acetone (−0.4), CO_2 (−0.2) and H_2O (−0.1), indicating the occurrence of product inhibition by competing for adsorption on the catalytic sites. The C-C coupling was proposed as rate determining elementary step in the ketonization mechanism. While suppression of the reaction rate by the ketonization products was not permanent in this particular case, others have observed irreversible deactivation by H_2O when using $Ce_{0.7}Ti_{0.3}O_x$ [22]. This was ascribed to competitive surface adsorption, hydrolysis of reaction intermediates or

* Corresponding author.
E-mail address: bert.sels@kuleuven.be (B.F. Sels).

https://doi.org/10.1016/j.apcatb.2021.121052
Received 21 October 2021; Received in revised form 20 December 2021; Accepted 28 December 2021
Available online 5 January 2022

disintegration of the active material under hydrothermal conditions. Depending on the specific substrate, catalyst and reactor system under investigation, relevant literature has not only shown different orders and strength of substrate adsorption and product inhibition, but also their ketonization temperature dependency (adsorption enthalpy) [13,23,24].

Related to this, the influence of the feedstock chain length on the substrate-surface interaction, and therefore ketonization kinetics, has been studied in detail. As a rule, the reaction is slower when starting from longer carboxylic acids. For ketonization of C_2-C_4 carboxylic acids on Ru/TiO_2 [25] and HZSM-5 [26] catalysts, this has been linked to the difference in contribution of the adsorption entropy. For instance, a value of − 198 J/mol.K was calculated for acetic acid on Ru/TiO_2, while this increased to − 178 J/mol.K for butyric acid. This relationship was also found for other kinetic and thermodynamic parameters such as the true activation energy, activation entropy and activation enthalpy. In contrast, no difference was found in the adsorption enthalpy values when varying the ketonization feedstock. These findings imply that the substrate-surface interaction is not governed by the alkyl tail, but rather by adsorption of the polar acid group. Additionally, it is clear that the transition state requires more space in the immediate surroundings of the active sites during C-C bond formation of carboxylic acid molecules with a higher carbon number. As a result, this steric hindrance slows down the rate determining step for longer carboxylic acids, increasing the energy demand.

To describe the rate determining step of C_2-C_4 gas-phase ketonization, Langmuir-Hinshelwood (LH) kinetic models have been proposed the most. Depending on the specific conditions, these may in- or exclude inhibition by one of the reaction products, while adsorption of all relevant species is generally described by competition for the same catalytic site [2]. The few existing liquid phase ketonization studies have mainly focused on C-C coupling of acetic acid in aqueous reaction media. To maintain liquid phase conditions, very high reaction pressures (up to 190 bar) have been reported when operating at a high ketonization temperature (340 °C) [27]. In contrast, Ru/TiO_2, TiO_2/C and Ru/TiO_2/C catalysts have been used at 180 °C in various solvents such as hexane, N-Methyl-2-pyrrolidone and water [28]. The highest ketonization activity was achieved with Ru/TiO_2/C in the organic media, reportedly due to the hydrophobic nature of this support material limiting the amount of water inhibition. Related to the latter, others have also observed increased activity and/or stability of more hydrophobic ketonization catalysts such as HF treated TiO_2 [29] and ZrO_2/C [30] when using water as ketonization solvent. The most striking example was reported by Aranda-Pérez et al. where a 5% Ru/TiO_2 catalyst was only active for aqueous phase acetic acid ketonization when the TiO_2 crystal phase was rutile [31]. Both anatase and P25 (anatase-rutile mixture) TiO_2 phases were inactive, in contrast to the experiments carried out in hexane. Additionally, catalyst phase changes may occur due to the hydrothermal ketonization conditions, as has been shown for amorphous $La_xZr_yO_z$ catalysts undergoing crystallization [32]. Interestingly, the reaction of C_2 carboxylic acid has been studied theoretically in both gas and liquid aqueous phase using a ZrO_2 catalyst [33]. The ketonization kinetics in water were best described by an Eley-Rideal (ER) mechanism, with a lower ketonization rate compared to the gas phase. In this reaction medium, the amount of available acid-base pairs for ketonization was reduced significantly as a consequence of competitive adsorption by H_2O, which can furthermore also hydroxylate the active sites and take part in proton transfer reactions during the elementary steps of the ketonization mechanism (Grotthuss mechanism). In conclusion, the reaction environment surrounding the active surface is noticeably more complicated for liquid phase ketonization reactions.

Detailed investigation of the liquid phase reaction kinetics for C_{12}-C_{18} carboxylic acid using heterogenous catalysts is currently missing in this research field. It must be noted that the kinetics of liquid phase C-C coupling of stearic acid, in dodecane solvent and absence of catalyst addition, has been published [34]. The observed catalytic ketonization activity was assigned to the stainless steel reactor wall in this particular case. Shorter reactions (3 h) starting from low fatty acid concentrations (0.15 M) resulted in high selectivity to the 18-pentatriacontanone product. However, fatty acid decarboxylation became the dominant reaction pathway for longer reactions (96 h) at higher temperatures and substrate loadings (1.75 M), considerably reducing the ketonization selectivity. Low conversion (20–30%) and selectivity (18–22%) values have also been reported for ketonization of stearic acid when using ZrO_2 catalysts in dodecane in hydrogen atmosphere (40 bar) at 260 °C [35].

This concise overview reveals some of the recent progress made to better understand the mechanism and kinetics of short-chain carboxylic acid ketonization in the gas phase. However, no kinetic study has been performed on the (liquid phase) catalytic ketonization of fatty acids, to the best of our knowledge. Evidently, this information is required for the design and development of future ketonization biorefinery processes for the synthesis of bio-based waxes and derivatives. As a result, the key goal of this work is to describe and model the liquid phase kinetics of fatty acid ketonization. Hereto, the activity of two commercial TiO_2 catalysts (anatase (A) and rutile (R)) is investigated kinetically in a (semi-)batch reactor in dodecane solvent. These reaction data are used to develop a kinetic model, describing the reaction of the catalysis, which is linked to the physicochemical surface properties of the catalysts. Furthermore, the influence of substrate properties (such as chain length), reactor mode and operating conditions are explored to test and validate the kinetic model. Possible deactivation effects by ketonization products are studied explicitly. Finally, this study compares these results to earlier developed kinetic concepts derived from the short-chain gas phase studies, and discusses both similarities and differences.

2. Experimental

2.1. Chemicals & materials

2.1.1. Substrates

The following fatty acid substrates were used in this study: lauric acid (98%, Sigma Aldrich), myristic acid (98%, Sigma Aldrich), palmitic acid (98%, Acros Organics), stearic acid (97%, Acros Organics) and arachidic acid (99%, Fisher Scientific).

2.1.2. Products

All ketone products were purchased from TCI Europe: laurone (12-tricosanone, 95%), myristone (14-heptacosanone, 95%), palmitone (16-hentriacontanone, 95%) and stearone (18-pentatriacontanone, 95%).

2.1.3. Catalysts

The commercial TiO_2 catalysts under investigation were kindly provided by Venator (Hombikat M211, anatase (A) and Hombikat Mikrorutil, rutile (R)).

2.1.4. Other chemicals

The eicosane standard (99%), n-dodecane reaction solvent (99%) and chloroform analysis solvent (HPLC grade) were purchased from Acros Organics. The N-methyl-N-(trimethylsilyl)trifluoroacetamide (MSTFA, 98.5%) derivatization agent for trimethylsilylation was purchased from Sigma Aldrich.

2.2. Catalyst characterization

2.2.1. X-ray diffraction

A Stadi P Combi diffractometer instrument (STOE), capable of high-throughput analysis, was used to perform the powder X-ray diffraction measurements. The data were collected in transmission mode (CuKα1 (λ = 1.54 Å) radiation, Ge (111) monochromator) using an image plate position sensitive detector. The applied scanning range for 2θ was 5–60 °.

2.2.2. Scanning electron microscopy

Scanning electron microscopy images were collected by a JSM-6010 JV microscope (JEOL) at 10 kV accelerating voltage. Prior to imaging, a gold coating was applied to the catalyst materials using JSC-1300 sputter equipment (JEOL).

2.2.3. Nitrogen physisorption

The catalyst powders were first pre-treated in a constant N_2-flow at 300 °C for 5 h. Afterwards, the N_2 isotherms were recorded at − 196 °C by a Tristar II 3020 instrument (Micromeritics). Catalyst surface areas and pore sizes were quantified by BET and BJH analysis, respectively.

2.2.4. Temperature-programmed desorption

First, pellets (250–500 μm) were made from the original TiO_2 powder samples and loaded into a quartz tube inside a customized plug flow fixed bed measurement system. Quartz wool was used to keep the catalyst sample in place, while pelletizing ensures gas plug flow at constant pressure while minimizing the risk of clogging, tunneling and pressure build-up and losses as would be the risk for the powder samples. For ammonia TPD, the pre-treatment step consisted of heating at 5 °C/min to 400 °C in He. This temperature was maintained for 1 h, after which the catalyst sample was cooled to 150 °C. Then, NH_3 was allowed to adsorb for 30 min, followed by additional flushing with He for 30 min to remove physisorbed NH_3. Desorption of gasses ($m/z = 16$ for NH_3) was analyzed from 150 °C to 800 °C (10 °C/min ramp). For CO_2 ($m/z = 44$), the experimental procedure was identical, except lowering the adsorption temperature to 50 °C. All datapoints were collected by a Omnistar quadrupole mass spectrometer (Pfeiffer), and data analysis (deconvolution) was carried out using OriginPro software package.

2.2.5. Pyridine FT-IR spectroscopy

Self-supporting wafers of the TiO_2 materials were first pre-treated at 400 °C and 1 mbar vacuum for 1 h. To evaluate the potential presence of Lewis (L) and Brønsted (B) acid sites, the TiO_2 wafers were then saturated with pyridine probe at 50 °C (25 mbar pyridine vapor). Prior to data collection at 150 °C, the samples were degassed at 150, 250 or 350 °C. Using 256 scans per spectrum and 2 cm^{-1} resolution, analysis was carried out on a Nicolet 6700 spectrometer with DTGS detector. A Lewis acid extinction coefficients (ε(L)) value of 1.63 cm/μmol was used [36,37].

2.2.6. UV–vis diffuse reflectance spectroscopy

The TiO_2 samples were pelletized between 250−500 μm and put into a quartz U-tube with UV−vis transparent window. Pre-treatment was carried out in N_2 flow at 300 °C (5 °C/min heating rate) for 1 h. Afterwards, data recording was performed at room temperature in nitrogen atmosphere for wavenumber values ranging from 4000 to 50,000 cm^{-1}. All spectra were corrected for background signals using dried $BaSO_4$ pellets as reference. A Cary 5000 UV−vis−NIR spectrophotometer (Agilent) was used for all measurements. The final results are displayed by the Kubelka−Munk function.

2.3. Ketonization reaction

2.3.1. Reaction procedure

For the ketonization reactions, the fatty acid substrate, n-dodecane solvent and TiO_2 catalyst (wt% loading expressed as $m_{catalyst}/m_{substrate}$) were added into a 100 ml Parr reactor. Inertization of the reaction atmosphere was ensured by repeating the same N_2 flushing procedure (10 bar N_2, stirring at 600 rpm for 1.5 min, evacuating headspace) three times. The desired ketonization temperature was then reached by heating from room temperature. With the experimental set-up, the reactor is entirely surrounded by the heating mantle which fully encompasses the reactor, including the head space. Semi-batch ketonization experiments at constant pressure were defined by addition of a continuous N_2 flow through the liquid phase during reaction. The input of this flow was controlled by BRIGHT modules (Bronkhorst), with back pressure regulators maintaining a constant reactor pressure. The gasses at the reactor outlet were passed through a condenser set at 5 °C, without losing any fatty acids or ketones. After ketonization, the system was cooled to 50 °C and depressurized before further analysis.

2.3.2. Product analysis

For product analysis, 0.5 g of internal standard (eicosane) was added and the reaction medium was stirred for 10 min. Then 3 ml chloroform was added to 1 ml sample. To remove any remaining TiO_2 from this mixture, centrifugation was carried out for 15 min at 3500 rpm. The supernatant was derivatised with MSTFA (5 times molar excess) at 60 °C for 1 h to silylate any remaining fatty acid molecules. Using N_2 carrier gas, a 6890 gas chromatography instrument (Agilent) with HP-5 column (30 m, 0.32 mm internal diameter, 0.25 μm film thickness) and flame ionization detector (320 °C) was used to analyze the composition of the reaction mixture (1 μl injection volume, 10:1 split ratio, 300 °C injection temperature). Starting from 60 °C, the oven temperature was increased to 190 °C (10 °C/min heating rate), from 190 °C to 200 °C (1 °C/min ramp) and from 200 °C to 310 °C at 5 °C/min. The final temperature was held for 15 min. Standard calibration curves, obtained with the analytical grade fatty acids and ketones, were used to quantify these results. A 5973 gas chromatography-mass spectrometry instrument (Agilent) with HP-5 ms column (25 m, 0.25 mm internal diameter, 0.25 μm film thickness) was used to identify any unknown compounds.

2.3.3. Kinetic analysis

For the kinetic experiments, the reaction time was set to $t = 0$ once the target temperature was reached. Any conversion of substrate to products that occurred during the heating window was accounted for by appropriately adjusting the C_0 compound concentrations at t_0. For all kinetic experiments, the total substrate conversion values were kept below 53%. Carbon mass balances were > 97% for all experiments. Parameter estimation by linear regression analysis of reaction data was done by OriginPro software. For the Langmuir-Hinshelwood kinetic models, multiple non-linear regression was performed with XLSTAT software by Addinsoft [38] using a numerical iterative Levenberg-Marquardt algorithm to minimize the objective function (sum of square of errors). A confidence level of 95% was used throughout this study for statistical analysis.

3. Results and discussion

3.1. Catalyst characterization

The two commercial TiO_2 catalysts were characterized prior to screening their ketonization activity. The crystal phases of both materials were verified via PXRD, indicating pure anatase (A) and rutile (R) phases (Fig. 1A). For A TiO_2, the dominant crystal surface was (101), situated at a 2θ value of 26 degrees. For R TiO_2, the (110) surface was most abundant (with a 2θ value of 28 degrees) [39]. Using the Scherrer equation, apparent primary crystallite (domain) sizes of 7.8 and 11.6 nm were obtained for A and R, respectively. These values are in line with the primary crystallite size as, provided by the manufacturers. The DRS UV–vis measurements also accord to the presence of these crystal structures as band gap energies of 3.3 and 3.05 eV were found (Kubelka-Munk theory) for anatase and rutile TiO_2, respectively (Supporting information, Fig. S1A). This is in good agreement with typical reported values for these different crystal phases [40]. Scanning electron microscopy images show for both materials that the primary (nanosized) crystals aggregate into larger heterogeneously (micrometer) sized particles (Fig. 1B and Fig. 1C). The BET surface area, total pore volume and pore diameter parameters were determined via N_2 physisorption with 266 m^2/g, 0.36 cm^3 /g and 5.1 nm for A, and 77 m^2/g, 0.63 cm^3 /g and 38 nm for R TiO_2, respectively.

The acid-base properties were determined by temperature

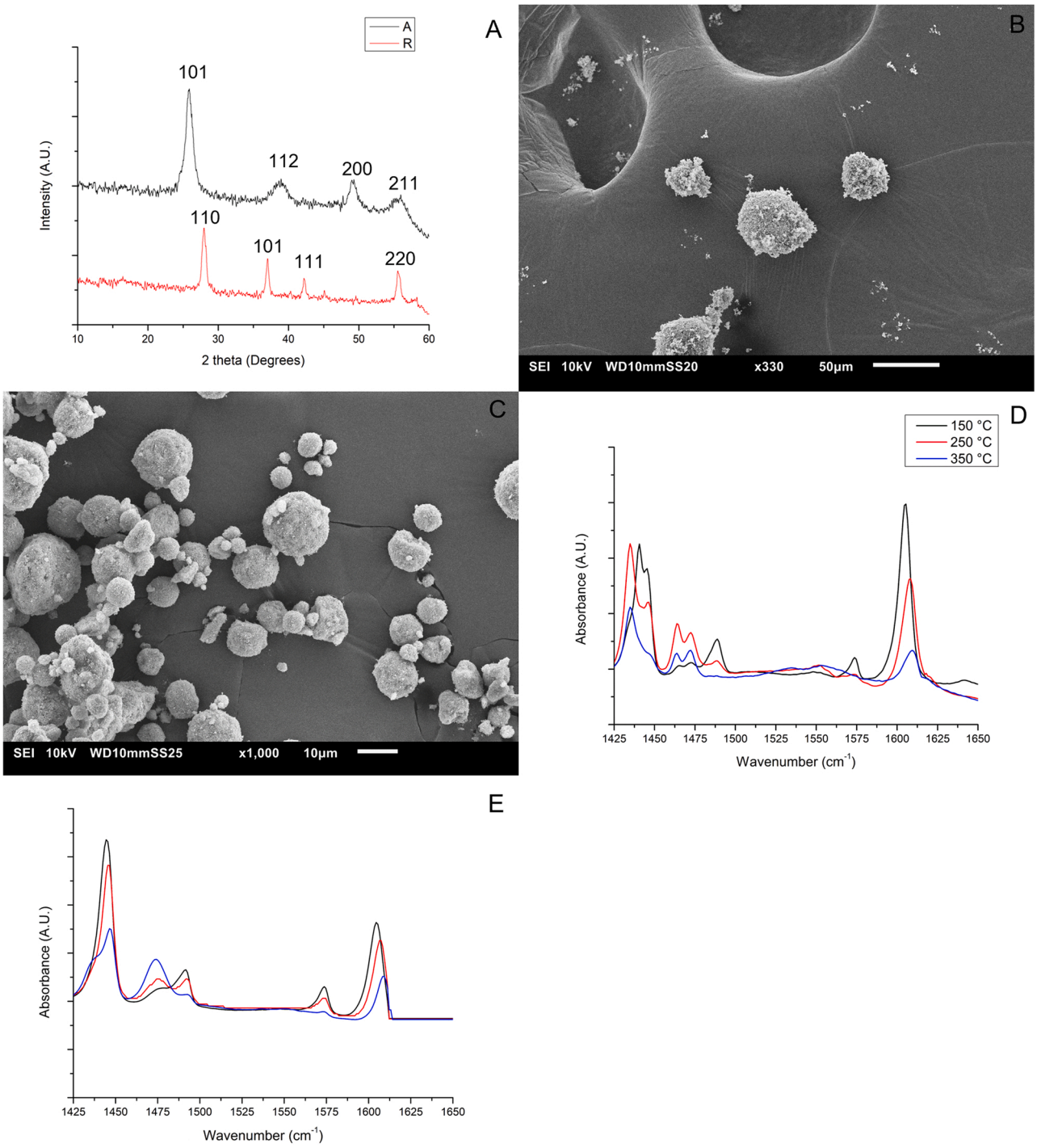

Fig. 1. PXRD of anatase (A) and rutile (R) (A); SEM of R (B) and A (C); Pyridine IR measurements at 150, 250 and 350 °C for A TiO_2 (D) and R TiO_2 (E).

programmed desorption (TPD) of NH_3 and CO_2 probes, and by FT-IR spectroscopy with pyridine as probe molecule. The broad signals of the TPD measurements were deconvoluted to distinguish acid-base sites with different strength (Supporting information, Fig. S1B-S1E). For NH_3 TPD analysis of anatase TiO_2, desorption maxima were found at 238, 317 and 427 °C, which were assigned to weak (16%), medium (53%) and strong (31%) acid sites, respectively. For rutile TiO_2, these maxima occurred at higher desorption temperatures of 270 °C (32%), 401 °C (58%) and 611 °C (10%). The desorption of NH_3 base at lower temperatures for A indicates weaker bonding of the probe molecule with the Lewis acid surface sites, and thus lower acid site strength compared to the active sites of R. Next, CO_2 was used as acid probe molecule to determine the basicity of both catalysts. The use of this probe is particularly interesting for the ketonization reaction, as CO_2 is also one of the reaction products. For A TiO_2, two broad desorption signals between 50 and 225 °C (70%) and 425–800 °C (30%) were observed, indicating the presence of weaker and stronger Lewis base sites, respectively. The R catalyst mainly showed a broad signal between 50 and 300 °C (90%), and two smaller signals between 450 and 600 °C (5%) and 625–800 °C (5%), indicating that A TiO_2 has a higher percentage of basic sites which interact more strongly with the CO_2 probe. Integration of the CO_2 signal revealed that the total basicity is higher for A TiO_2, when expressed in terms of both catalyst surface area and weight.

Pyridine probe FT-IR spectroscopy was performed to discriminate between Lewis and Brønsted acid sites. Rutile TiO_2 showed characteristic Lewis acid site absorption bands at 1441, 1489, 1575 and 1605 cm^{-1} (Fig. 1E). Given no signals at 1545 and 1635 cm^{-1}, absence of Brønsted acid sites can be assumed. The quantity and strength of the coordinatively unsaturated Ti^{x+} surface species was investigated by determining the amount of chemisorbed pyridine probe at different temperatures. Quantification of the FT-IR analysis resulted in acid site density values of 1.73, 1.61 and 0.72 μmol/m^2 at 150, 250 and 350 °C, respectively. At the highest temperature, 42% of the chemisorbed pyridine remained on the catalyst surface, indicating presence of strong Lewis acid sites. Similarly, A TiO_2 is characterized by Lewis acid absorption bands at 1445, 1492, 1575 and 1606 cm^{-1}, with no significant amounts of Brønsted acid sites (Fig. 1D). For this catalyst, the acid site density values at 150, 250 and 350 °C were 1.22, 0.86 and 0.42 μmol/m^2, respectively. Compared to rutile, this indicates weaker interaction between the chemisorbed pyridine probe and the Lewis acid surface sites on anatase, as more pyridine desorbed at the higher temperatures. Overall, R has a higher acid site density on a surface area basis, while A has a higher amount of acid sites per catalyst weight. In summary, both commercial catalysts are pure phase amphoteric TiO_2 materials with distinct (Lewis) acid-base properties (Table 1).

3.2. Fatty acid ketonization and mass transfer

An initial study of the ketonization activity of both TiO_2 catalysts was performed in the liquid phase using lauric acid (C12:0) as a model fatty acid compound (Fig. 2). Since H_2O and CO_2 are formed during reaction, the mass yield of C_{23} laurone is limited to a maximum value of 84.5% at full lauric acid conversion. Dodecane was used as inert reaction solvent, allowing variations in initial substrate and product concentrations.

Fig. 3A displays the evolution of lauric acid (LA) concentration over time during ketonization with 10 wt% TiO_2 catalysts (powder form) in a closed batch reactor operating at 340 °C and autogenous pressure (9.5 bar) with a stirring rate of 600 rpm. The results clearly show that R has a higher (initial) ketonization activity for a similar catalyst weight. Under these conditions, the ketonization selectivity was always ≥ 98% for both catalysts.

Before conducting further kinetic experiments, it is important to exclude that any diffusion issues are determining this observed activity. To determine whether these results represent intrinsic activity in the chemical regime, the potential presence of mass transfer limitations was studied. External mass transfer limitations were investigated by varying the stirring rate between 75 and 800 rpm (Fig. 3B). It can be seen that increasing the stirring rate from 75 to 300 rpm resulted in a minor conversion rate increase for both catalysts, viz. 12% for A and 4% for R, respectively. A further increase from 300 rpm to 600–800 rpm again

Table 1
Summary of characterization results of anatase (A) and rutile (R) TiO_2 catalysts used in this work.

Catalyst property	Anatase (A)	Rutile (R)	R/A ratio
Primary crystallite size (nm)[a]	7.8	12.8	NA
Band gap (eV)	3.3	3.05	0.92
BET surface area (m^2/g)	266	77	0.29
Pore volume (cm^3/g)	0.36	0.63	NA
Pore diameter (nm)	5.1	38	NA
Lewis acidity (μmol/g) at 150 °C	324	133	0.41
Lewis acidity (μmol/m^2) at 150 °C	1.22	1.73	1.42
Lewis acidity (μmol/m^2) at 250 °C	0.86	1.61	1.87
Lewis acidity (μmol/m^2) at 350 °C	0.42	0.72	1.71
Bronsted acidity (μmol/g) at 150 °C	< 1	< 1	NA
Relative acidity[b] (%)	100	273	2.73
Relative basicity[b] (%)	100	62	0.62

NA: Not applicable.
[a] Based on XRD.
[b] Based on total integrated TPD signal area per surface area of catalyst.

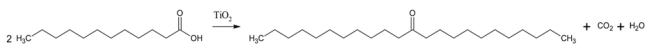

Fig. 2. Ketonization of lauric acid to laurone, CO_2 and H_2O with a TiO_2 catalyst.

(slightly) increased the reaction rates by 3%. There was no difference in the 600–800 rpm range and therefore 600 rpm was chosen as a suitable stirring rate in this study to guarantee exclusion of external mass transfer limitations, which will also be evidenced further when determining the activation energy values. Next, internal mass transfer limitations were investigated using the Weisz-Prater Criterion (C_{WP}), assuming spherical and isothermal particles (Supporting Information). The intrinsic observed reaction rates were taken from the initial C(t) part, equaling 9.0 * 10^{-4} and 50 * 10^{-4} M/m^2h for A and R TiO_2, respectively (or 2.5 and 4.0 g/g_{cat}h in terms of weight). The true catalyst densities are 3.9 and 4.2 g/cm^3 for A and R, respectively, as provided by the manufacturer via pycnometer measurement. Based on analysis of the SEM images (Supporting Information, Fig. S2), a particle radius value of 30 μm was chosen as a reasonable upper limit to avoid any underestimation of C_{WP} for both catalysts. The bulk diffusivity of the substrate was calculated by the Wilke-Chang equation and verified with reported values of similar reaction systems (Supporting Information) [41,42]. For an initial substrate loading of 15 mmol, the concentration of lauric acid at the catalyst surface is set equal to the bulk concentration since external mass limitations were excluded earlier. As a final result, the calculated effective diffusivity values are 7.26 * 10^{-9} and 7.34 * 10^{-9} m^2/s for A and R, respectively, which ultimately results in C_{WP} values of 6.6 * 10^{-3} and 1.4 * 10^{-2} (Supporting Information). Since both values are $<<1$, it can be stated that no internal mass transfer limitations are present under the applied reaction conditions, which implies that the experimental data presented under these conditions are governed by the catalytic reactions occurring in the chemical regime.

Based on the C(t) profiles of Fig. 3A, it was found that a second order reaction model best described the experimental data (Supporting Information, Fig. S3 and Table S1). Physically, the ketonization reaction may adhere to a second order model since the bimolecular coupling requires two adsorbed carboxylic acids at the catalyst surface. It must be noted that the experimental data do not exclude the possibility of a first order model ($p < 0.05$). From a physical standpoint, this may apply for ketonization when acid molecules are readily adsorbed on the catalyst surface, awaiting the adsorption of a second molecule on an adjacent active site for the C-C coupling. In this case, the ketonization rate may be linearly proportional to the substrate concentration. The latter may be more probable at higher substrate concentrations. The slopes of the second order models in Fig. S3 were used to determine the second order rate constants of A ($0.014 \pm 0.002 M^{-1}min^{-1}$) and R ($0.076 \pm 0.005 M^{-1}min^{-1}$). Finally, the Thiele modulus (φ_{pn}) and reaction efficiency (η) values were calculated (Supporting Information). Based on the experimental data, the Thiele modulus values are 1.1 * 10^{-3} and 2.3 * 10^{-3} for A and R TiO_2, respectively. These correspond with 99.9% reaction efficiency for both catalysts, confirming again that the reaction rate is indeed determined by the catalytic reaction, and the data are not interfered by mass transfer limitation phenomena.

3.3. Kinetics of fatty acid ketonization in liquid phase

3.3.1. Impact of substrate and catalyst loading

Both the initial substrate concentration and catalyst loading were varied to determine their impact on the ketonization activity. First, the initial lauric acid loading was varied between 0 and 30 mmol (Fig. 4). The general R(C_0) trend is rather similar for both TiO_2 catalysts, alluding to the existence of two regimes. At lower lauric acid concentrations, there is a larger impact of substrate concentration on the ketonization rate, while the reaction rate curves start to flatten for higher

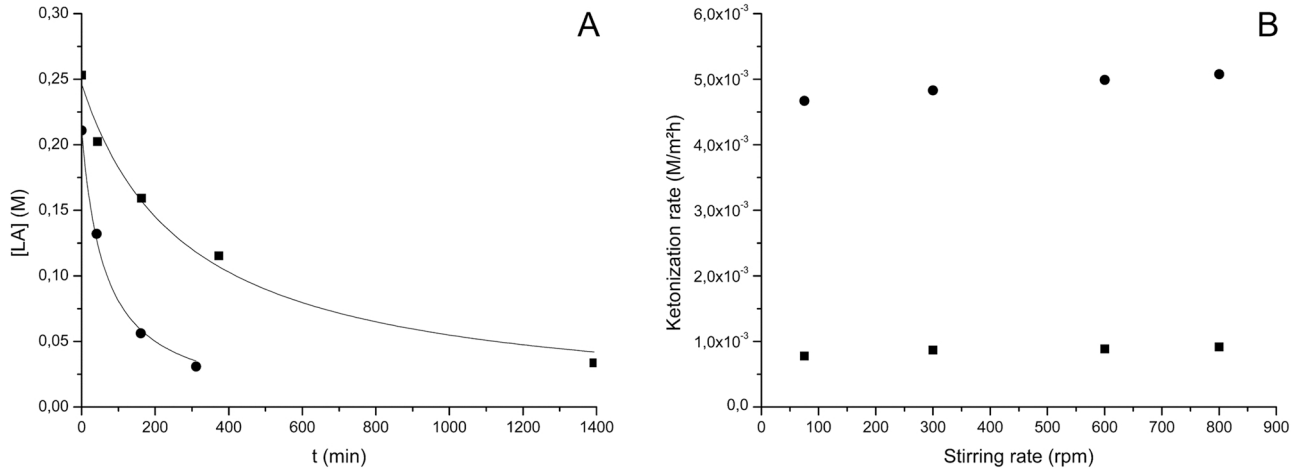

Fig. 3. C(t) plot for ketonization of lauric acid with A (■) and R (●) TiO_2, with full lines representing second order reaction fitting. Reaction conditions: 15 mmol LA – 40 g DD – 0.3 g TiO_2 – 340 °C – 600 rpm – autogenous pressure (A); Ketonization rate of lauric acid in function of stirring rate. Reaction conditions: 15 mmol LA –40 g DD – 0.3 g TiO_2 – 340 °C – 45 min – autogenous pressure (B).

concentrations. From these data, the observed reaction orders n were determined in the applied concentration ranges for both catalysts by linearization of the power law (Eq. (1)):

$$R_{obs} = k_{obs}[LA]^n \quad (1)$$

with R_{obs} the observed reaction rate (in M/m^2h), k_{obs} the observed rate constant, $[LA]$ the lauric acid concentration and n the observed reaction order. For A TiO_2, the overall observed reaction order is 0.39 ± 0.02 (Fig. S4A). For the R catalyst, the n value is significantly higher at 0.55 ± 0.07 (Fig. S4B). These observed fractional orders indicate a lauric acid concentration range for the bimolecular ketonization reaction in which a state of saturation of catalytic active sites is approached for high fatty acid concentrations, where the ketonization rate will no longer increase for higher initial lauric acid loadings. As stated in the introduction, this has also been observed by others for C_2-C_4 gas-phase ketonization reactions. Furthermore, the observed orders differ significantly between both catalysts, suggesting a difference in substrate-surface interaction. An initial substrate loading of 15 mmol lauric acid was chosen for further investigation as it grants sufficient possibilities to vary catalyst and product loadings in the next paragraphs, while taking into account compound solubilities and allowing the ketonization rates to vary up to at least an order of magnitude.

The influence of the catalyst loading was investigated in the range of 2.5–20 wt% at a constant initial lauric acid concentration (Fig. S5). For both catalysts, the ketonization rate (expressed on surface area basis) was reduced for a higher loading of 20 wt%. This reduction was more severe in the case of the R catalyst (39%) compared to the A material (14% reduction). For both catalysts it may indicate an upper limit of substrate adsorption, flocculation/aggregation of catalyst particles with loss of added surface area, higher viscosity of the reaction medium, and related to that limited mass transfer or other phenomena which reduce the activity per added surface area for higher catalyst loadings. The R TiO_2 catalyst may be more prone to the flocculation/aggregation effects. Furthermore, its higher intrinsic turnover rate is also accompanied by a higher sensitivity to product inhibition (Section 3.3.3), which may become more pertinent at the highest catalyst loading of 20 wt% due to fast initial product formation. The catalyst loading of 10 wt% was therefore selected for further kinetic study.

As a reference, thermal ketonization experiments were also carried out in absence of any TiO_2 catalyst (Supporting Information, Fig. S6). After a total time of 90 min (including heating phase), the total lauric acid conversion only reached 4.4% with 69% selectivity to the laurone product, equaling a 10 mM/h initial conversion rate and 3.6 mM/h ketone productivity. In comparison, the experiments carried out with A TiO_2 always showed $>$ 98% ketone selectivity, with initial conversion rate values of 22–113 mM/h for 2.5–20 wt% catalyst loading, equaling

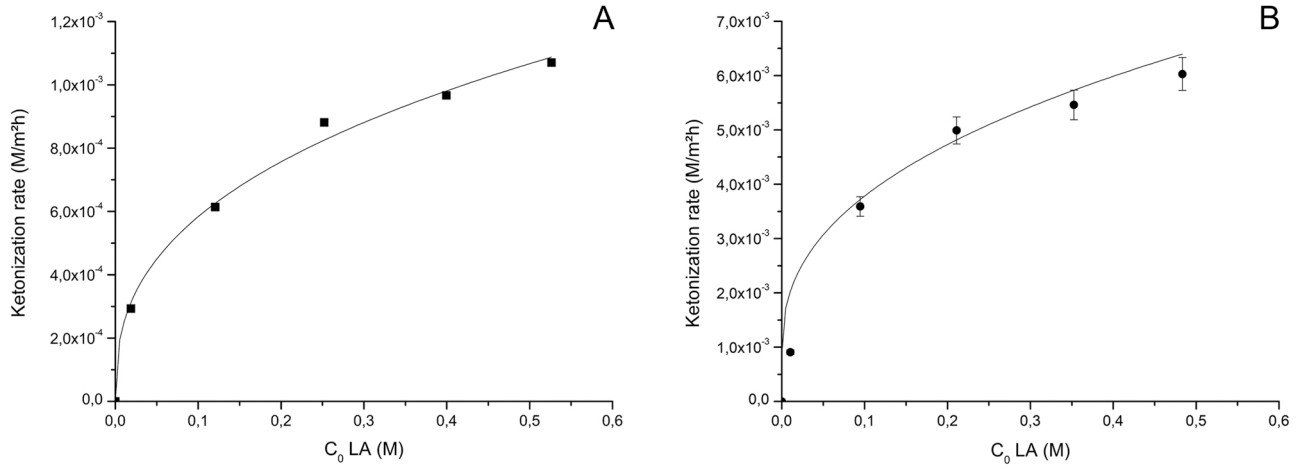

Fig. 4. Ketonization rate in function of initial lauric acid concentration for A (A) and R (B) catalysts. The full lines represent fitting of the power law equation $R_{obs} = k_{obs}[LA]^n$ with n = 0.39 for A, and n = 0.55 for R. Reaction conditions: 40 g DD – 0.3 g TiO_2 – 340 °C – 45 min - 600 rpm – autogenous pressure.

11–57 mM/h ketone productivity rates. In other words, the ketone productivity increased by a factor of 3.1–16 compared to the thermal ketonization experiment without formation of unwanted side products. For the R TiO_2 catalyst, these lauric acid conversion and ketone productivity values are even higher, with 4.1–17 times higher ketone productivity for 2.5–20 wt% catalyst loading. For a longer total time of 270 min in absence of catalyst, the lauric acid conversion was 16.1% with 61% selectivity for laurone. These values are significantly lower than those obtained in the presence of either A or R catalyst. For example, already after 210 min the total lauric acid conversion values were 43% and 80% for 10 wt% loading of A and R, respectively, with full selectivity to the desired ketone product. Our data unambiguously show that the presence of the heterogenous catalyst is preferred to achieve fast ketonization reactions with high product yields and selectivity.

3.3.2. Temperature dependency of liquid phase catalytic ketonization

The influence of the reaction temperature was studied between 300 and 340 °C to determine the (apparent) activation energy, observed enthalpy, entropy and Gibbs free energy of activation. As shown in Fig. S7, increasing the reaction temperature from 300°C to 340°C significantly increased the ketonization rate for both catalysts, revealing an exponential relationship in agreement with Arrhenius law. From these results, apparent activation energies of 137 ± 7 kJ and 117 ± 5 kJ/mol were determined for A and R, respectively. These values for liquid phase catalysis are in good agreement with other reported values for gas-phase ketonization, viz. 105 and 116 kJ/mol for 2-methyl-butanoic acid and pentanoic acid on ZrO_2 [43], 132 kJ/mol for acetic acid on KOH treated ZrO_2 [44], 92–124 kJ/mol on isolated ZrOH [45] and 124 kJ/mol for propanoic acid on Zn-Cr mixed oxide [46]. Higher values have also been published, such as 185 kJ/mol for C_2 acid ketonization with Ru/TiO_2 [17], 160 kJ/mol for C-C coupling of pure C_{16} acid on K_2O/TiO_2 [47] and 177 kJ/mol for palm fatty acid distillate ketonization on TiO_2 in liquid phase [6]. The substrate and catalyst, but also the reactor system and operational conditions clearly impact the observed activation energy values. Our results conclude that under the applied reaction conditions in a batch reactor, the activation energy values differ significantly between both TiO_2 phases and that ketonization of fatty acids is kinetically more favorable on the rutile phase, compared to anatase TiO_2.

The temperature dependent conversion data were used to get more insight into the thermodynamics of the transition state. In Fig. 5, the Eyring-Polanyi equation of transition state theory was plotted to identify the contribution of the activation enthalpy and entropy to the Gibbs free energy of activation for lauric acid ketonization. The slopes of both curves were used to calculate $\Delta H^{\ddagger}$, while $\Delta S^{\ddagger}$ can be derived from the intercepts (Supporting Information). For A TiO_2, the $\Delta H^{\ddagger}$, $\Delta S^{\ddagger}$ and $\Delta G^{\ddagger}$ parameters for the rate determining step (C-C coupling, see kinetic

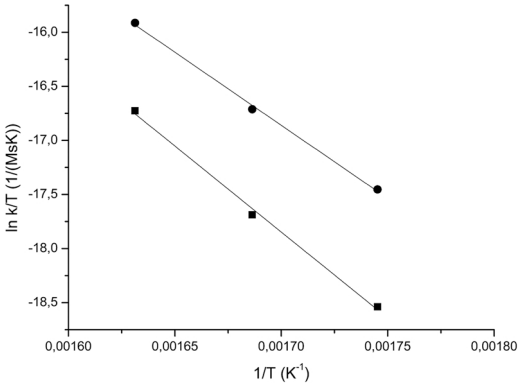

Fig. 5. Eyring-Polanyi plot to determine $\Delta H^{\ddagger}$, $\Delta S^{\ddagger}$ and $\Delta G^{\ddagger}$ for lauric acid coupling on A (■) (adj. $R^2 = 0.99$, F-value = 335, p-value = 0.03) and R (●) (adj. $R^2 = 0.99$, F-value = 613, p-value = 0.03) TiO_2.

Table 2
Summary of Arrhenius and Eyring-Polanyi analysis for lauric acid ketonization on A and R TiO_2 at 340 °C.

	Anatase (A)		Rutile (R)		P-value*
	Value	95% CI	Value	95% CI	
$E_{a,obs}$ (kJ/mol)	137 ± 7	129,145	117 ± 5	111,123	0.02
$\Delta H^{\ddagger}$ (kJ/mol)	132 ± 7	124,140	112 ± 5	106,118	0.02
$\Delta S^{\ddagger}$ (J/mol. K)	-121 ± 19	-99,– 143	-147 ± 22	-122,– 172	0.19
$\Delta G^{\ddagger}$ (kJ/mol)	206 ± 16	188,224	203 ± 15	186,220	0.82

*2 sample t-test.

model paragraph) are 137 ± 7 kJ/mol, -121 ± 19 J/mol.K and 204 ± 16 kJ/mol, respectively, at 340 °C (Table 2). For R, these values are 112 ± 5 kJ/mol, -147 ± 22 J/mol.K and 203 ± 15 kJ/mol, respectively, for the rate determining step. These data indicate that for A and R TiO_2, the enthalpy term has a larger contribution to the Gibbs free energy of activation than the entropy for the studied ketonization temperature range. Furthermore, the enthalpy terms differ significantly between both catalysts, which is not the case for the activation entropy. The formation of the transition state (TS) is characterized by a loss of entropy, which agrees with the associative nature of the bimolecular C-C coupling of carboxylic acids to produce an activated complex. Some $\Delta S^{\ddagger}$ values have been reported for gas-phase ketonization before, such as -90 and -135 J/mol.K for pentanoic and 2-methylbutanoic acid on ZrO_2, for example [43]. Oppositely, positive $\Delta S^{\ddagger}$ values have also been stated for C_2-C_4 acid ketonization [25], although this possibility of a TS with more degrees of freedom is counterintuitive. A combination of kinetic experiments and DFT calculations using anatase TiO_2 for acetic, propanoic and butyric acid coupling revealed $\Delta G^{\ddagger}$ values ranging between 166 and 176 kJ/mol at 250 °. For the reaction of acetic acid, $\Delta H^{\ddagger}$ was 137 kJ/mol with $\Delta S^{\ddagger}$ equal to -56 J/mol.K at 230 °C [13]. When using ZrO_2, $\Delta G^{\ddagger}$ values varied between 157 and 168 kJ/mol for the different acid substrates [14]. Our data for the liquid phase ketonization of fatty acids is largely in accordance with the reports for gas-phase ketonization of shorter acids.

3.3.3. Product inhibitory effects

Prior to the construction of a kinetic model for both catalysts, the possibility of product inhibition was examined in more detail. This includes all three ketonization products, namely ketone, H_2O and CO_2. First, the potential effect of the ketone product was assessed experimentally by adding pure C_{27} myristone (14-heptacosanone, $CH_3(CH_2)_{12}C{=}O(CH_2)_{12}CH_3$), the ketonization product of myristic acid ($C_{14:0}$), at the start of reaction. Up to 8.2 mmol ketone was added, covering the entire conversion range of lauric acid since the maximum theoretical yield of laurone is 7.5 mmol when 15 mmol lauric acid substrate is used. Myristone is used as an analog model for laurone to reduce analytical complexity, assuming that its potential impact is comparable to that of laurone due to their very high degree of similarity. Furthermore, it is assumed that the ketone is entirely present in the liquid phase under reaction conditions, given its 440–450 °C boiling point. As can be derived from Fig. 6 A and Fig. 6B, there is indeed a significant negative impact of the ketone product on the ketonization rate, albeit to a different degree for both TiO_2 catalysts. For A, the ketonization rate drops gradually for increasing ketone concentrations, showing a 15% decrease in activity in presence of 0.08 M myristone. Any additional concentration increase of ketone did not further lower the ketonization rate. Using a power law equation, a minor but significant negative experimental reaction order of -0.07 ± 0.01 was calculated for the ketone product in this entire concentration range (Fig. S8A). In contrast, a much larger negative impact was found for R TiO_2, for which a low initial myristone concentration already resulted in a significantly steep decline of the acid conversion

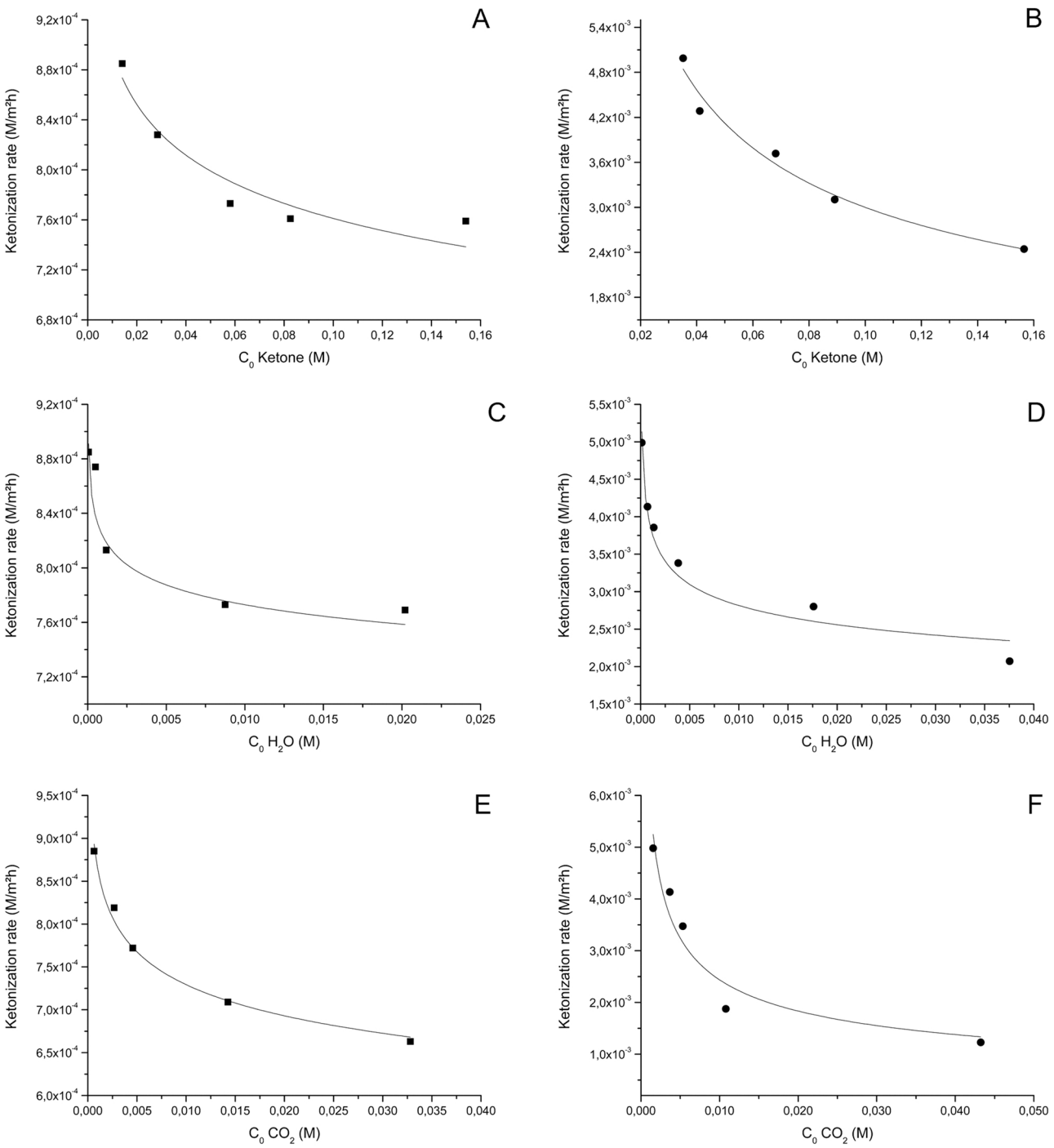

Fig. 6. Ketonization rate in function of initial myristone concentration for A (A) and R (B) TiO_2. Ketonization rate in function of initial effective water concentration for A (C) and R (D) TiO_2. Ketonization rate in function of initial effective CO_2 concentration for A (E) and R (F) TiO_2. The full lines represent fitting of the power law equations with the experimentally derived observed product reaction orders. Reaction conditions: 15 mmol LA – 40 g DD – 0.3 g TiO_2 – 340 °C - 45 min - 600 rpm – autogenous pressure.

rate. Furthermore, the negative trend is continued for higher concentrations, albeit to a lesser extent than the initial activity drop. For instance, an initial myristone concentration of 0.15 M led to a more than halving of the reaction rate. From these results, a negative order of -0.46 ± 0.03 was determined for the R catalyst, indicating a significantly higher sensitivity to ketone inhibition compared to A (Supporting Information, Fig. S8B). These observations suggest competitive adsorption of the ketone product on the active sites via its carbonyl group, reducing their availability for carboxylic acid substrate molecules and the ketonization reaction.

Besides ketone, also the impact of H_2O on the conversion rate was studied. Here liquid distilled water, in the range of up to 167 mmol, was added at the start of reaction. Note that 15 mmol is the maximum theoretical yield of H_2O at full lauric acid conversion. Compared to the ketone product, the kinetic effect is more complex to describe as the majority of the added water will appear in the head space as vapor during reaction due to the high ketonization temperature. The interaction between water and the reaction solvent should also be considered in this case as water is poorly soluble in dodecane. Therefore, the effective initial water concentration in the liquid phase was estimated based on

calculations that combine the observed total system pressure and extrapolation of literature data regarding the solubility of water in dodecane at elevated temperatures [48]. Depending on the initial loading, the molar fraction of water in the liquid dodecane phase is only between 0.36% and 1.2% at 340 °C. As a result, the effective initial water concentration at reaction temperature varies approximately up to 37 mM (while adding a maximum of 3.1 M, not taking into account vapor pressure and solubility factors). Fig. 6C and Fig. 6D present the effect of water on the ketonization rate for both catalysts in terms of the initial calculated effective concentrations. The experiments show a significant negative impact on the ketonization rate for both materials, although the trend and strength of the inhibitory effect is different. The A catalyst undergoes a drop in conversion rate in the presence of water, but the reaction rate stabilizes at 87% of the initial activity for effective water concentrations of 9 mM and higher as an increase to 20 mM did not have a further negative impact (Fig. 6D). Analysis of these experiments reveals a minor (but significant) -0.03 ± 0.005 observed reaction order for water (Fig. S8C). The water inhibitory effect was also observed for R, although for this catalyst there is a continuous decline of the ketonization rate for the whole concentration range tested (Fig. 6E). In contrast to A TiO_2, the ketonization rate still decreases above effective water concentrations of 9 mM. For instance, the reaction rate is reduced by 44% at 18 mM and by 59% at 37 mM (highest initial water concentration). The overall observed reaction order of water for this entire concentration range is -0.16 ± 0.02 for the R catalyst (Supporting information, Fig. S8D). This difference in trend and strength of water inhibition show a more pronounced sensitivity for the more active R material. For both catalysts, the origin of the water inhibition effect is more complex than that of the ketone product, since more factors could contribute to its negative impact on the catalytic activity. Firstly, competitive adsorption of water on the active surface sites is possible via the water hydroxyl groups. Secondly, the H_2O molecules (formed during ketonization) could also partake in forward and reverse (de)protonation elementary reaction steps [33]. Thirdly, the catalyst surface may also become the subject of hydrothermal breakdown (e.g. TiO_2 phase transitions or sintering with reduction of surface area) under the ketonization conditions, which can impact its catalytic performance (see Supporting Information for post-reaction SEM analysis, Fig. S9). The R catalyst remains the most active TiO_2 material, even though it is more susceptible to the inhibitory effect of the H_2O ketonization by-product.

Thirdly, the effect of CO_2 was determined experimentally by initially pressurizing the batch reactor with external CO_2 (up to 12 bar) at room temperature before heating. The results are shown in Fig. 6E and Fig. 6F, and it must be noted first that reference experiments under inert N_2 atmosphere at various pressures were performed to rule out any overall pressure effect. We found no effect of the total system pressure on the rate of reaction for the studied pressure range. As such, the observations in Fig. 6 are directly related to the presence of CO_2. As was the case for water, the initial CO_2 concentration in the liquid phase was estimated to be able to calculate its effective kinetic inhibitory effect on the ketonization catalysis (since the largest part will be in the head space). This estimation uses extrapolation of available literature data regarding the solubility of CO_2 in liquid hydrocarbons at elevated temperatures and pressures [49]. The molar fraction of CO_2 in dodecane at 340 °C is around 4.4–9.1%, depending on the total system pressure, and was used to determine the effective initial CO_2 concentrations in the liquid phase, which maximizes at 43 mM (for initial pressures up to 12 bar). Note that 140 mM is the maximum theoretical concentration of CO_2 at full lauric acid conversion if 100% of the formed CO_2 is solubilized in the liquid phase reaction medium. For A TiO_2, the ketonization rate declines continuously, with a 25% reduction of the reaction rate at 32 mM CO_2. A similar but more severe trend can be observed for R TiO_2, as its ketonization activity is reduced by 75% for 43 mM CO_2. Analysis of these experimental data reveals negative observed reaction orders of -0.07 ± 0.004 and -0.46 ± 0.06 for the A and R catalysts, respectively (Fig. S8D and S8E). The negative impact of carbon dioxide may be attributed to competitive adsorption on the surface sites. Although the environments surrounding the catalysts are different than during liquid phase reaction in dodecane, the CO_2 TPD experiments have shown that CO_2 desorption still occurs above the reaction temperature of 340 °C for both catalysts. Surface carbonates may be formed, or bicarbonates in co-presence of water, deactivating the TiO_2 surfaces for further ketonization [50,51].

Since there are no reports on these inhibitory effects for liquid phase ketonization, direct comparison with literature data cannot be made. However, there is mentioning of a recent patent application on continuous liquid phase fatty acid ketonization with TiO_2 that employs the CO_2 by-product as carrier gas [47], which seems inadvisable based on our data. In the referenced work, water is stripped from the condensed phase by the recycled CO_2 to counteract active site inhibition by H_2O. Here, only the latter has been taken into account, while our study shows that the inhibition of CO_2 could at least be as important, if not more.

These experiments unambiguously show that inhibition from all products should be considered when performing fatty acid ketonization reactions in the liquid phase. Furthermore, the more active R catalyst is most prone to such inhibition (compared to A TiO_2) for all reaction products, which is demonstrated experimentally for the first time in this work for liquid phase fatty acid ketonization (Table S2). In conclusion to this part and by using the experimentally derived reaction orders, the observed ketonization rates can be expressed as power laws according to Eq. (2) and Eq. (3) for A and R TiO_2, respectively.

$$R_{A,obs} = k_{A,obs}[C_{Acid}]^{0.39}[C_{ketone}]^{-0.07}[C_{H2O}]^{-0.03}[C_{CO2}]^{-0.07} \quad (2)$$

$$R_{R,obs} = k_{R,obs}[C_{Acid}]^{0.55}[C_{ketone}]^{-0.46}[C_{H2O}]^{-0.16}[C_{CO2}]^{-0.46} \quad (3)$$

3.3.4. Irreversibility of liquid phase ketonization and the re-ketonization side reaction

In a recent gas phase study, it has been shown that under specific conditions, the reaction products could undergo the reverse ketonization reaction to the original acid substrates [52]. Additionally, a diketone intermediate may be formed as a result of the re-ketonization side reaction between a carboxylic acid and ketone molecule [53]. This condensation intermediate can either decompose back to the original acids in case of homo-ketonization, or create new ketones during cross-ketonization. Therefore, it is important to consider and investigate the possibilities of equilibrium and re-ketonization for liquid phase fatty acid ketonization. Experiments arguing such equilibrium were described earlier in this contribution, and studied the impact of the inhibitory effect of the ketone product. When adding C_{27} myristone to the reaction mixture, significant equilibrium would have led to the formation of the C_{25} ketone cross-product. However, no such ketone was detected, indicating that at least in our conditions, re-ketonization does not occur. Furthermore, myristic acid was also not observed in these experiments. To further corroborate the irreversibility of ketonization, an additional experiment was carried out in the presence of C_{35} stearone (18-pentatriacontanone). The reaction was monitored for longer reaction times, viz. 4.5 h, and higher concentration of stearone was added (lauric acid and stearone were added in a 1:1 wt ratio). Although these modified conditions are more favorable to enable cross-coupling, no C_{29} ketone (12-nonacosanone) cross-ketonization product or stearic acid were observed. From these experimental observations, it can be concluded that under the applied ketonization conditions, the liquid phase ketonization of fatty acids may be treated as an irreversible reaction. As a consequence, the following kinetic models exclusively include parameters related to the forward reaction.

3.3.5. Kinetic rate equation for liquid phase catalytic ketonization of fatty acids

A kinetic model was developed for both catalysts to gain further insight in the elemental steps of the liquid phase ketonization of fatty acids and its rate-determining step (RDS). Based on the good agreement

of our activation energy data with previous kinetic studies on gas-phase ketonization, the bimolecular C-C coupling of two adsorbed carboxylic acid (derived) species is proposed as the RDS on the catalyst surface (Eq. (8)). Furthermore, all three reaction products are assumed to compete for the same active surface site (*) (Eqs. (5–7)). Therefore, the elementary reaction steps taken into account are adsorption and desorption of substrate and products, and the C-C coupling of two activated substrates on the catalyst surface:

$$RCOOH + * \leftrightarrow RCOOH* \quad (4)$$

$$RCOR + * \leftrightarrow RCOR* \quad (5)$$

$$H_2O + * \leftrightarrow H_2O* \quad (6)$$

$$CO_2 + * \leftrightarrow CO_2* \quad (7)$$

$$RCOOH* + RCOOH* \rightarrow RCOR* + H_2O + CO_2 + * \quad (8)$$

As a result, a Langmuir-Hinshelwood (LH) kinetic model is obtained for the liquid phase ketonization reaction according to Eq. (9) (see Supporting Information for derivation):

$$R = k\frac{K_{Acid}^2 C_{Acid}^2}{\left(1 + K_{Acid}C_{Acid} + K_{ketone}C_{ketone} + K_{H2O}C_{H2O} + K_{CO2}C_{CO2}\right)^2} \quad (9)$$

with R the ketonization rate, k the rate constant of the surface reaction, K_x the equilibrium adsorption constants and C_x the liquid phase concentrations of acid, ketone, water and carbon dioxide. To determine the kinetic and thermodynamic k and K_i parameters, multiple non-linear regression was performed with XLSTAT software by Addinsoft [38] using a numerical iterative Levenberg-Marquardt algorithm to minimize the objective function (sum of square of errors). An overview of the results is given in Table 3, showing that all parameters are significantly different from zero.

First, they indicate a large difference in rate constant between both materials, as the k value for R is more than six times higher compared to A (on surface area basis). This corroborates the substantially higher intrinsic activity of R for ketonization of fatty acids. Secondly, a different degree of interaction of reagent and products is evident for both catalysts, since the adsorption constants not only significantly differ in absolute value, but also in relative order (see also Supporting Information). For A, the adsorption constants decrease in the order $CO_2 > H_2O$ = acid > ketone, whereas this series is altered to $CO_2 > H_2O >$ ketone = acid for R TiO_2. These observations clearly underscore the different sorption behavior of the TiO_2 surfaces under similar conditions, indicating different (surroundings of) active sites on the A and R surfaces. Notably, the significantly higher adsorption constants of ketone, H_2O and CO_2 on R are in good agreement with the product inhibition experiments. Stronger adsorption of these products on the active surface sites indeed lead to a stronger inhibition of the overall ketonization rate. It is thus apparent that the intrinsically higher conversion rate of R is simultaneously counteracted by its higher sensitivity to product inhibition by adsorption, which is less dominant for A.

While the numerical results of Table 3 cannot be compared due to the lack of available literature data on liquid phase fatty acid ketonization, it is valuable to discuss the general concepts that came out our data in comparison with previous kinetic studies, carried out in the gas phase for short-chain acids. Adsorption constants have been reported for C_2-C_4 acid ketonization on Ru/TiO_2 (P25) in the presence of a Cu/SiO_2 co-catalyst under H_2 atmosphere at 275–335 °C [25]. For reaction of butyric acid at 335 °C, the adsorption constant values were 0.102, 0.051, 0.003 and 0.002 $Torr^{-1}$ for acid, ketone, water and carbon dioxide, respectively. Stated otherwise, the ratios of the K values of the products in relation to the substrate equalled 0.5, 0.03 and 0.02 for ketone, water and carbon dioxide, respectively. In our case, these relative values are 0.19, 1.1 and 1.7 for the A catalyst, and 1.1, 7.5 and 15 for R TiO_2 (for same product order). Comparatively, the ketonization products seem to have a stronger binding tendency in the liquid-phase batch reaction, especially for the R catalyst. The high absolute values of the K parameters for H_2O and CO_2 are related to the low absolute concentrations of these compounds in the liquid phase under ketonization reaction conditions.

With these LH parameters, parity plots were constructed for A and R in Fig. 7. They present the correlation between the measured reaction rates (experimental work throughout this study) and the predicted ketonization rates, calculated based on the above developed LH model. In general, it can be stated that this kinetic model is in good agreement with the observed experimental results, while deviation is mostly observed for the higher H_2O and CO_2 concentrations, especially for the R catalyst. Nevertheless, the kinetic model correlations are satisfactory, especially when considering the complexity of the system due to the difficulty of determining exact concentrations of water and carbon dioxide in the condensed phase where the catalysis is actually taking place. Furthermore, interaction between these products in the reaction liquid or on the catalyst surface may not be discarded yet (formation of bicarbonates for example). The margins of error/uncertainty on these parameters reflect this complex system, which we have studied in detail for the first time. Future research should expand on these topics, as well as further expand the set of reaction conditions.

Comparison of the kinetic equation with those reported for gas phase ketonisation reveals several differences. Some of these LH models completely exclude product inhibition, whereas others introduce separate adsorption of the carboxylic acid substrate and ketonization products on different types of active sites [54]. As stated in the introduction part, an ER mechanism has also been suggested for the aqueous phase ZrO_2 catalyzed reaction of acetic acid [33]. In this ER mechanism, it is assumed that only one carboxylic acid is adsorbed and activated on the catalyst surface, which then directly undergoes the C-C coupling reaction with a second non-adsorbed carboxylic acid from the liquid phase. Such ER model cannot accurately describe our experimental results (Supporting information, Fig. S10 and Table S3), and we have shown the rate determining step to be the C-C coupling of two adsorbed acid species.

3.3.6. Ketonization activity of anatase (A) and rutile (R) TiO_2

This kinetic study clearly indicates significant differences between A and R with regard to their conversion rate (type and number of active

Table 3
Parameter estimation for lauric acid ketonization based on the Langmuir–Hinshelwood fitting of the experimental data.

	Anatase (A)		Rutile (R)		P-value*
	Value	95% CI	Value	95% CI	
$k(M/m^2h) * 10^{-3}$	1.3 ± 0.06	1.2,1.3	8.1 ± 0.001	7.7,8.6	$< 1 * 10^{-5}$
$K_{Acid}(M^{-1})$	19 ± 2.7	17,20	70 ± 19	62,78	$< 1 * 10^{-5}$
$K_{ketone}(M^{-1})$	3.6 ± 1.2	3.1,4.1	76 ± 24	65,86	$< 1 * 10^{-5}$
$K_{H2O}(M^{-1})$	20 ± 7.8	17,24	527 ± 169	454,599	$< 1 * 10^{-5}$
$K_{CO2}(M^{-1})$	32 ± 7.2	28,35	1028 ± 289	905,1152	$< 1 * 10^{-5}$

*2 sample t-test.

sites) and inhibition effects (sensitivity of the active sites). An earlier gas-phase study also revealed ketonization performance differences among these TiO_2 crystal phases, showing five times higher initial turnover rate of acetic acid for an anatase catalyst compared to the stronger acidic rutile TiO_2 [13]. These findings are opposite to our results, and were ascribed to two different factors. According to the authors, the specific crystal lattice distances between active Ti-Ti and Ti-O species of anatase are more suitable for adsorption of acetic acid in monodentate configuration, which was proposed as the reactive substrate form to undergo C-C coupling. Secondly, TS experiences increased stabilization on anatase, due to the intermediate strength of Lewis acid-base sites. Oppositely, the smaller $d_{Ti5c\text{-}Ti5c}$ of rutile results in a less favorable surface environment for the formation of TS, which is hindered sterically and stabilized less as a result of the stronger acidity of catalytic sites. Furthermore, acetic acid is preferentially adsorbed in bidentate mode on rutile, which was assumed to be a non-reactive spectator configuration. Interestingly and in sharp contrast, a very recent gas phase study found, as in our work, rutile TiO_2 to be more active than anatase for ketonization of acetic and propionic acid [55]. Here, the shorter intermolecular separation of two adsorbed carboxylate substrates on rutile was used as primary reasoning to explain its higher ketonization activity. The same was also proposed earlier for the liquid-phase reaction of C_2 acid, albeit with modified anatase and rutile TiO_2 catalysts by incorporating Ru metal [31]. In the latter, the batch ketonization reaction was carried out in water and hexane solvents using bifunctional 5% Ru/TiO_2 catalysts. The bifunctional rutile catalyst was characterized by a higher Lewis acid site density, a direct consequence of more favorable TiO_2 surface reduction by the Ru metal via hydrogen spillover compared to the anatase catalyst. According to the authors, this increased amount of and shorter distance between active Ti^{3+} Lewis acid sites improved the acetic acid conversion rate in hexane by 150–400% compared to anatase. Additionally, incorporation of Ru can also impact the surface acid site strength, This will in turn influence adsorption and desorption of ketonization substrates, intermediates and products, impacting the ketonization rate.

It must be noted that in these literature examples the catalysts and reaction systems are not always identical, which could implicate that the catalytic behavior of different TiO_2 materials is dissimilar in opposing systems. Clearly, our experimental and kinetic findings are more in line with the latter two studies, since the LH intrinsic rate constant k of the surface reaction is 6.4 times higher for R. Furthermore, the observed ketonization rate of lauric acid is 1.3–5.6 times higher on R, depending on how the reaction rate is expressed (Table 4). Therefore, our findings suggest that the higher Lewis acid site density, the smaller Ti-to-Ti distances or a combination of both are likely explanations for the higher reactivity of R TiO_2 for liquid-phase fatty acid ketonization.

Table 4
Comparison of observed ketonization rates expressed as function of weight, surface area and acidity between A and R TiO_2. Reaction conditions: 15 mmol LA – 40 g DD – 0.3 g TiO_2 – 340 °C - 45 min - 600 rpm – autogenous pressure.

Ketonization rate	Anatase (A)	Rutile (R)	R/A ratio
$R(g/g.h)$	2.5	4.0	1.6
$R(M/m^2.h) * 10^{-4}$	9.0	50	5.6
$R(M/\mu mol.h) * 10^{-4}$ (150 °C)	7.4	29	3.9
$R(M/\mu mol.h) * 10^{-4}$ (250 °C)	8.6	18	2.1
$R(M/\mu mol.h) * 10^{-4}$ (350 °C)	20	21.5	1.3

3.3.7. Mechanism

As stated in the introduction, current literature on the ketonization reaction mechanism suggests a pathway via a β-ketoacid intermediate with the C-C coupling as RDS [10]. Furthermore, the presence of α-H in one of the substrates is required to observe any ketonization activity. This hydrogen atom is abstracted from the substrate by the active surface, leading to the formation of an adsorbed 1-hydroxy enolate species which can interact with a second adsorbed substrate molecule [14]. Both the kinetic and thermodynamic parameters obtained in our kinetic study (E_a, $\Delta H^{\ddagger}$, $\Delta S^{\ddagger}$ and $\Delta G^{\ddagger}$) are in good agreement with those obtained in earlier (mechanistic) work [13,25], and our kinetic experimental data are consistent with the proposed Langmuir Hinshelwood C-C coupling model, allowing us to propose a β-ketoacid ketonization mechanism for liquid phase reaction of fatty acids, presented in Fig. 8 for lauric acid as an example.

First, two lauric acid molecules are adsorbed and activated on the catalytic surface by formation of a 1-hydroxy enolate and second adsorbed molecule after elementary steps such as α-H abstraction (a). Then, the rate-determining C-C coupling step occurs between the 1-hydroxy enolate and second adsorbed molecule, forming the β-ketoacid precursor (b). The latter undergoes elementary steps at the surface, resulting in the formation of the β-ketoacid intermediate and water is released from the surface as ketonization by-product (c). Ultimately, the intermediate dissociates, forming CO_2 by-product and the primary ketone product (d). After ketone desorption, the catalytic cycle is complete.

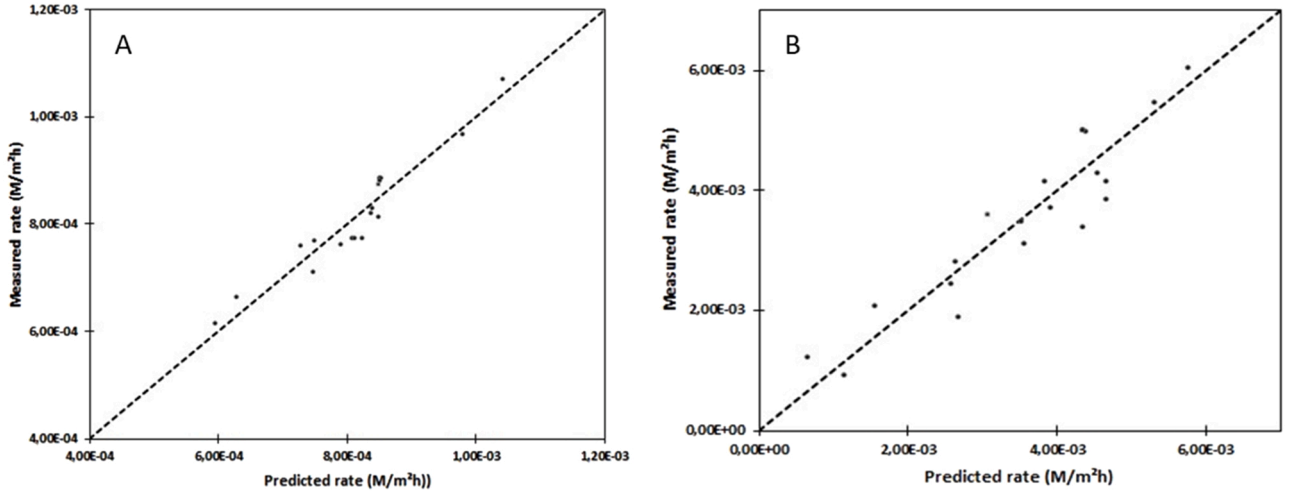

Fig. 7. Parity plots displaying correlation between measured experimental ketonization rates and reaction rates as predicted by LH model (Eq. (9)) for A (A) and R (B) catalysts.

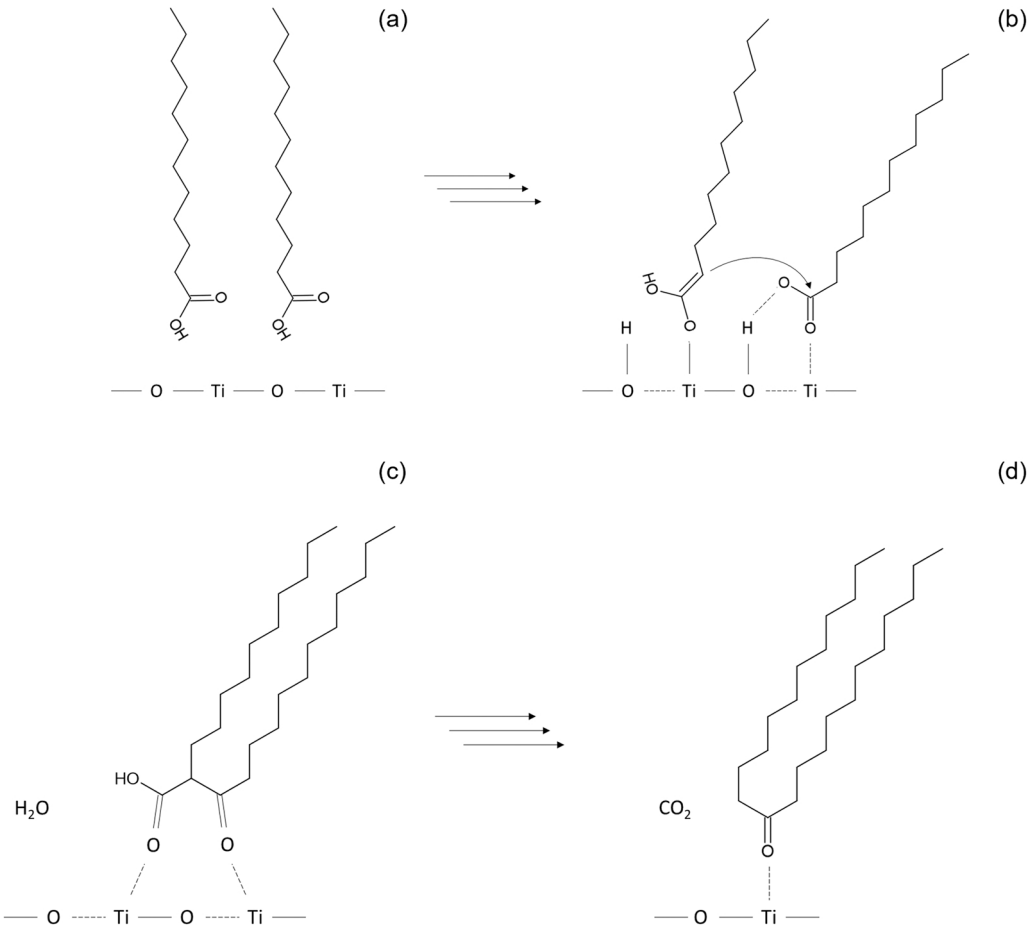

Fig. 8. Proposed mechanism for lauric acid ketonization on TiO_2 in liquid phase via β-ketoacid intermediate.

3.3.8. Effect of substrate chain length on ketonization rate

While lauric acid has been used as model compound up to this point, the influence of carbon chain length on the ketonization rate was also investigated by using saturated C_{14}-C_{20} fatty acid model compounds, namely myristic ($C_{14:0}$), palmitic ($C_{16:0}$), stearic ($C_{18:0}$) and arachidic acid ($C_{20:0}$). The same initial fatty acid loading of 15 mmol was used for all compounds, alongside identical reaction conditions, previously used for lauric acid. The results are summarized in Fig. 9A. As depicted in the graph, the ketonization rate is clearly affected by the fatty acid chain length. Shorter fatty acids show higher activity, which holds true for both TiO_2 catalysts. This observation is in line with previously reported general trends on gas-phase carboxylic acid coupling [2]. Additionally, this relationship seems to follow a rather linear trend for both catalysts, though the absolute degree of reduction is larger for R. For instance, the observed reaction rates are reduced by 29% and 57% for stearic acid when compared to lauric acid, for A and R, respectively.

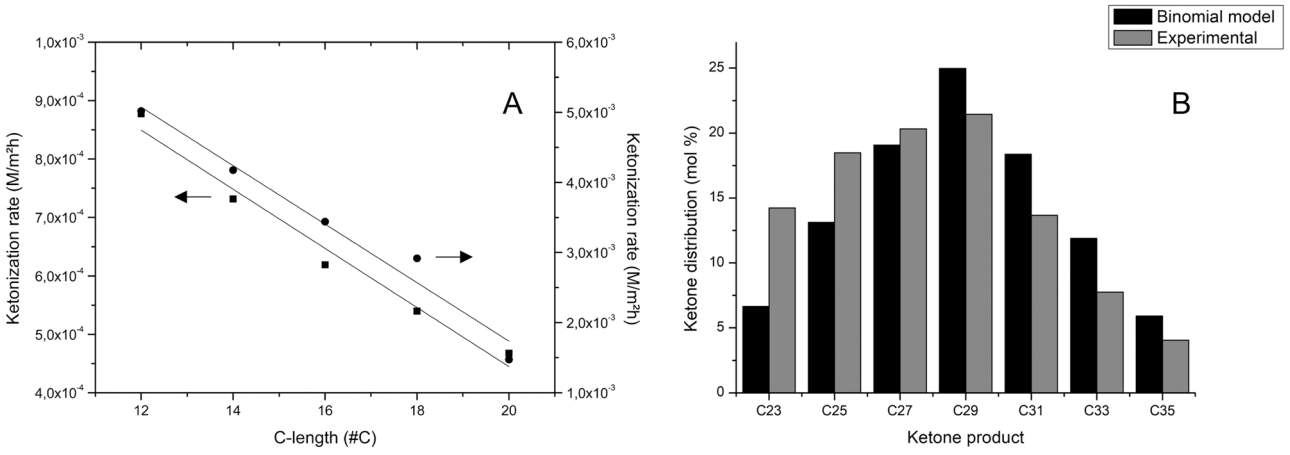

Fig. 9. Ketonization rate in function of fatty acid substrate chain length for A (■) and R (●) TiO_2. Reaction conditions: 15 mmol FFA – 40 g DD – 0.3 g TiO_2 – 340 °C - 45 min - 600 rpm – autogenous pressure (A). Experimental ketone product distribution after ketonization of an equimolar mixture of saturated C_{12}-C_{18} fatty acids in the presence of A TiO_2 vs. binomial model prediction. Reaction conditions: 15 mmol FFA – 40 g DD – 0.3 g TiO_2 – 340 °C - 45 min - 600 rpm – autogenous pressure (B).

To uncover the origin of the reduced ketonization rate for the longer fatty acids in the liquid phase, the coupling reaction of stearic acid (C18:0) was carried out with the A catalyst at different temperatures between 300 and 340 °C (Fig. S11). From these data an apparent activation energy of 148 ± 13 kJ/mol was determined (Arrhenius equation), which is higher (but not statistically significant) than the 137 ± 7 kJ/mol value observed for lauric acid. Secondly, the observed enthalpy, entropy and Gibbs free energy of activation values were also calculated for stearic acid. The $\Delta H^{\ddagger}$, $\Delta S^{\ddagger}$ and $\Delta G^{\ddagger}$ values were 143 ± 14 kJ/mol, − 107 ± 26 J/mol.K and 208 ± 20 kJ/mol kJ/mol at 340 °C, respectively, for the rate determining step (C-C coupling). These means are all higher compared to lauric acid at the same reaction temperature, although further study including broader temperature ranges is necessary to more accurately determine the underlying cause of the observed differences (Table 5).

Assuming constant temperature independent values for $\Delta H^{\ddagger}$ and $\Delta S^{\ddagger}$, $\Delta G^{\ddagger}$ values were plotted as a function of the reaction temperature between 300 and 550 °C (Fig. S12A). For lauric acid, there is a common intercept for the A and R TiO_2 graphs at 500 °C, indicating that the $\Delta G^{\ddagger}$ value becomes lower for the A catalyst at > 500 °C. Similarly, the $\Delta G^{\ddagger}$ value of SA becomes lower than that of LA for the A catalyst at 470 °C (Fig. S12B). For longer fatty acids,

the TS is bulkier and likely subjected to more steric hindrance, negatively impacting the formation of the C-C bond (RDS). This increases the energy barrier for the C-C coupling, and therefore the enthalpy and Gibbs free energy of activation values. In the β-ketoacid ketonization mechanism, it is possible that the nucleophilic character of the αC atom of the 1-hydroxy enolate is diminished by the stronger electron-donating properties of these longer alkyl chains, slowing down the RDS [13]. Regarding the entropy of activation, the higher entropy loss of shorter substrates may be a result of the general adsorption structure of the transition state during ketonization, as surface interaction occurs via the carbonyl groups. As this structure maintains rather similar for all substrates, the longer fatty acids have more carbon atom groups which are distanced further away from the catalyst surface, preserving a higher overall degree of freedom compared to carbon atoms of the shorter substrate chains, resulting in the lower entropy of activation (absolute value) [26]. Although not yet conclusive, our results suggest that the more active R catalyst may also be more prone to the effect of increased steric hindrance for longer fatty acids compared to A.

3.3.9. Fatty acid mixtures

Based on the findings of the previous section, and since biomass feedstock mainly consist of fatty acid mixtures, an equimolar mixture of saturated C_{12}-C_{18} fatty acids was used as ketonization substrate in the presence of the A catalyst. In this case, 7 different ketones can be formed with carbon chain lengths varying between 23 and 35 due to homo- and cross-ketonization of the 4 fatty acids. In Fig. 9B, the ketone distribution of the obtained product mixture is displayed after a reaction time of 45 min, and compared to the predicted outcome when a binomial model is used to describe the product distribution. For the latter, it is assumed that the probability of ketonization between two fatty acid molecules on the catalyst surface is equal for all substrates. However, the experimental results clearly show an enrichment of lower MW ketones (C_{23}-C_{27}) compared to the binomial model, whereas the experimental yield of C_{29}-C_{35} is lower than predicted. These findings for fatty acid mixtures may be linked to the results of the previous paragraph, showing higher ketonization reactivity for lower MW fatty acids, which has been reported before for gas phase ketonization reactions of short-chain carboxylic acids [2]. For longer reaction times, the partial conversion values of the fatty acids will approach each other, since the lower MW substrates will be depleted faster in the beginning, clearing the catalyst surface for (slower) ketonization of the remaining longer fatty acid molecules (Fig. S13).

Table 5
Summary of Arrhenius and Eyring-Polanyi model results for lauric and stearic acid ketonization on A TiO_2 at 340 °C.

	Lauric acid		Stearic acid		P-value*
	Value	95% CI	Value	95% CI	
$E_{a,obs}$ (kJ/mol)	137 ± 7	129,145	148 ± 13	132,164	0.26
$\Delta H^{\ddagger}$ (kJ/mol)	132 ± 7	124,140	143 ± 14	127,159	0.29
$\Delta S^{\ddagger}$ (J/mol. K)	-121 ± 19	-99,– 143	-107 ± 26	-76,– 136	0.49
$\Delta G^{\ddagger}$ (kJ/mol)	206 ± 16	188,224	208 ± 20	185,231	0.89

*2 sample t-test.

3.3.10. Impact of solvent

Up until now, all experiments in this study were performed in the liquid phase with dodecane as inert reaction solvent. While not shown here, we observed identical reaction rates when dodecane was replaced by hexadecane, indicating that there was no impact of the hydrocarbon chain length and/or boiling point. Additionally, batch experiments were also performed with pure lauric acid substrate without any added solvent, to investigate whether this reaction system might influence our previously observed activity patterns. Hereto, similar reaction conditions (temperature, catalyst loading, stirring rate) were chosen under autogenous pressure, and 40 g lauric acid substrate (0.2 mol) was used to provide adequate loading in the 100 ml batch reactor. The results of these experiments are shown in Table 6 (entries 1–6) for times up to 6 h (including heating phase) for both the A and R catalyst.

Similar to the solvent system, the ketonization selectivity was always very high (≥ 97%) for both catalysts. However, it is interesting to observe that here the A catalyst now shows a higher overall fatty acid conversion (and thus ketone yield) than R for all reaction times (entries 1–3 versus entries 4–6). This is opposed to our results of the solvent system, in which the R catalyst showed higher overall conversion of lauric acid. Furthermore, the absolute conversion values are much lower, with LA conversion values reaching 18% and 14% after 6 h for A and R, respectively. This indicates that the reaction rate is still higher for R when expressed on a surface area basis (by a factor of 1.5), as was the case for the solvent system (albeit it is now less pronounced). The activity patterns are clearly different for both reaction systems, which can be ascribed to the different reaction environment surrounding the catalyst and the substrate and product molecules. For the pure lauric acid system, the complexity rises even further than for the solvent system due to many (still) unknown factors such as solubility and concentrations of fatty acids, ketone, CO_2 and water in the intricate reaction medium. Related to this, it may also be linked to difference in sensitivity

Table 6
Solvent and pure liquid phase ketonization of lauric acid with A and R catalysts in batch and semi-batch modes.

Entry	Solvent	Mode	Catalyst	t (min)[a]	X (%)
1	/	Batch	A	90	9.2
2	/	Batch	A	180	12
3	/	Batch	A	360	18
4	/	Batch	R	90	4.1
5	/	Batch	R	180	8.6
6	/	Batch	R	360	14
7	Dodecane	Batch	A	90	28
8	Dodecane	Semi-batch	A	90	40
9	Dodecane	Batch	R	90	53
10	Dodecane	Semi-batch	R	90	93
11	/	Semi-batch	A	90	14
12	/	Semi-batch	R	90	8.4

Solvent reaction conditions: 15 mmol LA – 40 g DD – 0.3 g TiO_2 – 340 °C – 600 rpm. Pure reaction conditions: 0.2 mol LA – 4 g TiO_2 – 340 °C – 600 rpm. Batch experiments were conducted at autogenous pressure, semi-batch experiments were conducted at 10 bar with N_2 purging flow of 10 ml/min.

[a] Including heating phase.

to product inhibition for both catalysts, as shown throughout this work for the solvent system. Since the R catalyst is more prone to product inhibition, potentially higher product concentrations at the catalytic surface could be a cause of the observed experimental results. To the best of our knowledge, this difference in activity patterns is reported for the first time in this work, while no other studies have compared or investigated these topics for (fatty acid) ketonization. Future research on this topic may also include the use of other solvents to investigate the potential influence of solvent properties on liquid phase fatty acid ketonization.

3.3.11. Impact of venting

Lastly, lauric acid ketonization experiments were performed in semi-batch operation mode to determine whether the decrease in catalytic activity due to product inhibition could be limited (or even mitigated completely). Hereto, the same reactor was used, but with the addition of a continuous in-and-out flow of the gas phase. This was achieved by purging N_2 through the liquid reaction medium at constant pressure via a gas inlet tube connected to the mechanical stirrer. At the reactor outlet, a condenser is maintained at 5 °C, which prevents any liquid substrate or product loss. This implies continuous permanent removal of CO_2 and other gasses, while water, solvent, fatty acid and ketone are only temporarily removed (if applicable) as they are sent back into the reaction medium after contact with the condenser (and backflow to the reactor). Similar reaction conditions were used as before, with a constant pressure of 10 bar and a N_2 purging flow of 10 ml/min for the semi-batch experiments.

The results are shown in entries 7–12 of Table 6 for the A and R catalysts. Overall, they reveal a significant improvement of the conversion rate for both catalysts and reaction systems under semi-batch mode. For the solvent system, the conversion rate of lauric acid increased by 43% for the A catalyst (entries 7–8), while the R catalyst showed an even higher improvement of 75% (entries 9–10). These findings are in line with the difference in sensitivity to product inhibition for both catalysts, as it was shown before by our kinetic model that R is impacted more heavily by these phenomena. By continuous purging, the catalyst with the highest sensitivity showed the highest increase in catalytic activity. This trend is also present in the pure lauric acid liquid phase reactions, and to an even greater extent. Here, the ketonization rate of lauric acid increased by 48% for the A catalyst (entry 1 versus 11), while the R catalyst showed a remarkable improvement as the reaction rate was more than doubled (entry 4 versus 12). Clearly, removal of the reaction products is an efficient way to boost catalytic performance during liquid phase fatty acid ketonization.

4. Conclusions

In this work, the kinetics of liquid phase ketonization of C_{12}-C_{18} fatty acids over two TiO_2 catalysts, anatase and rutile, were studied for the first time. These high surface area catalysts, with Lewis acid-base amphoteric properties, both showed high selectivity towards the ketone product. It was found that the R catalyst, with a higher Lewis acid site density, had a significantly higher intrinsic ketonization activity for lauric acid coupling compared to A, in addition to a lower observed activation energy. The observed reaction order values of lauric acid indicated a chemical regime in which the catalytic sites approach a state of substrate saturation for higher concentrations of fatty acid. Our kinetic experiments showed that the more active R catalyst was also more prone to product inhibition of water, ketone and carbon dioxide due to competitive adsorption of these reaction products on the active surface sites. This product inhibition becomes important for solvent-less reaction, for which A showed the highest overall conversion rate. We have proposed a strategy to counter this product inhibition by CO_2 (and partly water) via their continuous removal with inert gas purging, enabling drastic improvement of the conversion rates.

Based on our experimental findings, a kinetic LH model was developed for both catalysts. Besides highlighting the importance of adsorption/desorption of substrate and product molecules on the active surface, the kinetic models indicate that the C-C coupling elementary step is rate determining in the liquid phase ketonization reaction mechanism of fatty acids. The ketonization activity of the TiO_2 catalysts is likely determined by a combination of the Lewis acid site density and the crystal lattice distances between active Ti species. Related to the latter, steric effects could potentially negatively impact the C-C bond formation for the longer fatty acids, increasing the energy barrier for TS at the active surface. This lowers the ketonization reactivity of the longer substrates, which is more pronounced for the R catalyst, in line with its shorter Ti-to-Ti distances compared to A. As a result, shorter ketones are enriched in the product mixture at early stages of the reaction when starting from equimolar fatty acid substrate mixtures.

CRediT authorship contribution statement

Bert Boekaerts: Conceptualization, Formal analysis, Investigation, Methodology, Validation, Visualization, Writing – original draft. **Ward Lorenz**: Conceptualization, Investigation, Validation. **Joost Van Aelst**: Conceptualization, Supervision, Writing – review & editing. **Bert Sels**: Conceptualization, Writing – review & editing, Supervision, Funding acquisition.

Declaration of Competing Interest

The authors declare that they have no known competing financial interests or personal relationships that could have appeared to influence the work reported in this paper.

Acknowledgements

B.B. acknowledges the Research Foundation-Flanders (FWO) for a Ph.D. Fellowship (strategic basic research - SB). J.V.A. acknowledges funding from the Industrial Research Fund KU Leuven (IOF fellow). B.S. acknowledges VLAIO for the Catalisti FISCH-ICON Biowax Project. We thank Venator for providing the catalyst materials.

Appendix A. Supporting information

Supplementary data associated with this article can be found in the online version at doi:10.1016/j.apcatb.2021.121052.

References

[1] M. Renz, Ketonization of carboxylic acids by decarboxylation: mechanism and scope, Eur. J. Org. Chem. 2005 (6) (2005) 979–988.
[2] B. Boekaerts, B.F. Sels, Catalytic advancements in carboxylic acid ketonization and its perspectives on biomass valorisation, Appl. Catal. B Environ. 283 (2021), 119607.
[3] J. Weber, et al., Effect of metal oxide redox state in red mud catalysts on ketonization of fast pyrolysis oil derived oxygenates, Appl. Catal. B Environ. (2018) 241.
[4] H. Jahangiri, et al., Zirconia catalysed acetic acid ketonisation for pre-treatment of biomass fast pyrolysis vapours, Catal. Sci. Technol. 8 (4) (2018) 1134–1141.
[5] A. Palizdar, S.M. Sadrameli, Catalytic upgrading of beech wood pyrolysis oil over iron- and zinc-promoted hierarchical MFI zeolites, Fuel 264 (2020), 116813.
[6] B. Boekaerts, et al., Assessment of the environmental sustainability of solvent-less fatty acid ketonization to bio-based ketones for wax emulsion applications, Green Chem. 23 (18) (2021) 7137–7161.
[7] F. Stewart Ray, L. Dunson Debra, Temperature-switching Materials Having Improved Strength and Thermal Properties, BAY MATERIALS LLC, 2010.
[8] M. Kettunen et al., Simultaneous Production of Base Oil and Fuel Components from Renewable Feedstock, NESTE OIL OYJ: EP, 2014.
[9] T.N. Pham, et al., Ketonization of carboxylic acids: mechanisms, catalysts, and implications for biomass conversion, ACS Catal. 3 (11) (2013) 2456–2473.
[10] A.V. Ignatchenko, Multiscale approach for the optimization of ketones production from carboxylic acids by the decarboxylative ketonization reaction, Catal. Today 338 (2019) 3–17.
[11] R. Kumar, et al., Ketonization of oxygenated hydrocarbons on metal oxide based catalysts, Catal. Today 302 (2018) 16–49.

[12] A. Pulido, et al., Ketonic decarboxylation reaction mechanism: a combined experimental and DFT study, ChemSusChem 6 (1) (2013) 141–151.
[13] S. Wang, E. Iglesia, Experimental and theoretical assessment of the mechanism and site requirements for ketonization of carboxylic acids on oxides, J. Catal. 345 (2017) 183–206.
[14] S. Wang, E. Iglesia, Experimental and theoretical evidence for the reactivity of bound intermediates in ketonization of carboxylic acids and consequences of acid–base properties of oxide catalysts, J. Phys. Chem. C 121 (33) (2017) 18030–18046.
[15] S.T. Almutairi, E.F. Kozhevnikova, I.V. Kozhevnikov, Ketonisation of acetic acid on metal oxides: catalyst activity, stability and mechanistic insights, Appl. Catal. A Gen. 565 (2018) 135–145.
[16] A.V. Ignatchenko, et al., Ab initio study of the mechanism of carboxylic acids cross-ketonization on monoclinic zirconia via condensation to beta-keto acids followed by decarboxylation, Mol. Catal. 441 (2017) 35–62.
[17] T.N. Pham, D. Shi, D.E. Resasco, Kinetics and mechanism of ketonization of acetic acid on Ru/TiO2 catalyst, Top. Catal. 57 (6) (2014) 706–714.
[18] A.D. Murkute, J.E. Jackson, D.J. Miller, Supported mesoporous solid base catalysts for condensation of carboxylic acids, J. Catal. 278 (2) (2011) 189–199.
[19] K. Kulyk, et al., Kinetics of valeric acid ketonization and ketenization in catalytic pyrolysis on nanosized SiO2, γ-Al2O3, CeO2/SiO2, Al2O3/SiO2 and TiO2/SiO2, ChemPhysChem 18 (14) (2017) 1943–1955.
[20] C.A. Gaertner, et al., Catalytic coupling of carboxylic acids by ketonization as a processing step in biomass conversion, J. Catal. 266 (1) (2009) 71–78.
[21] S. Ding, et al., Ketonization of propionic acid to 3-pentanone over CexZr1–xO2 catalysts: the importance of acid–base balance, Ind. Eng. Chem. Res. 57 (50) (2018) 17086–17096.
[22] F. Lu, et al., Promotional effect of Ti doping on the ketonization of acetic acid over a CeO2 catalyst, RSC Adv. 7 (36) (2017) 22017–22026.
[23] S.S. Jewur, J.C. Kuriacose, Influence of products and pretreatments on the ketonisation of acetic acid over iron oxide, J. Res. Inst. Catal. Hokkaido Univ. 24 (2) (1977) 73–82.
[24] A. Gumidyala, T. Sooknoi, S. Crossley, Selective ketonization of acetic acid over HZSM-5: the importance of acyl species and the influence of water, J. Catal. 340 (2016) 76–84.
[25] T.N. Pham, D. Shi, D.E. Resasco, Reaction kinetics and mechanism of ketonization of aliphatic carboxylic acids with different carbon chain lengths over Ru/TiO2 catalyst, J. Catal. 314 (2014) 149–158.
[26] J. Cao, et al., Conversion of C2–4 carboxylic acids to hydrocarbons on HZSM-5: effect of carbon chain length, Ind. Eng. Chem. Res. 58 (24) (2019) 10307–10316.
[27] K. Wu, et al., ZrMn oxides for aqueous-phase ketonization of acetic acid: effect of crystal and porosity, Chem. Asian J. 13 (9) (2018) 1180–1186.
[28] T. Pham, et al., Aqueous-phase ketonization of acetic acid over Ru/TiO2/carbon catalysts, J. Catal. 295 (2012) 169–178.
[29] A. Fernández-Arroyo, et al., High {0 0 1} faceted TiO2 nanoparticles for the valorization of oxygenated compounds present in aqueous biomass-derived feedstocks, J. Catal. 358 (2018) 266–276.
[30] K. Wu, et al., Carbon promoted ZrO2 catalysts for aqueous-phase ketonization of acetic acid, ACS Sustain. Chem. Eng. 5 (4) (2017) 3509–3516.
[31] N. Aranda-Pérez, et al., Enhanced activity and stability of Ru-TiO2 rutile for liquid phase ketonization, Appl. Catal. A Gen. 531 (2017) 106–118.
[32] J.A. Lopez-Ruiz, et al., Enhanced hydrothermal stability and catalytic activity of LaxZryOz mixed oxides for the ketonization of acetic acid in the aqueous condensed phase, ACS Catal. 7 (10) (2017) 6400–6412.
[33] Q. Cai, et al., Aqueous-phase acetic acid ketonization over monoclinic zirconia, ACS Catal. 8 (1) (2018) 488–502.
[34] D.Y. Murzin, et al., Ketonization kinetics of stearic acid, React. Kinet. Mech. Catal. 126 (2) (2019) 601–610.
[35] S. Foraita, et al., Impact of the oxygen defects and the hydrogen concentration on the surface of tetragonal and monoclinic ZrO2 on the reduction rates of stearic acid on Ni/ZrO2, Chem. Eur. J. 21 (6) (2015) 2423–2434.
[36] M. Barreau, X. Courtois, F. Can, FT-IR spectroscopy study of HNCO adsorption and hydrolysis over oxide-based samples dedicated to deNOx processes, Appl. Catal. A Gen. 552 (2018) 147–153.
[37] M. Tamura, K.-i Shimizu, A. Satsuma, Comprehensive IR study on acid/base properties of metal oxides, Appl. Catal. A Gen. 433–434 (2012) 135–145.
[38] Addinsoft, XLSTAT statistical and data analysis solution, 2020: New York, USA.
[39] H. Yin, et al., Hydrothermal synthesis of nanosized anatase and rutile TiO2 using amorphous phase TiO2, J. Mater. Chem. 11 (6) (2001) 1694–1703.
[40] C. Maheu, et al., UPS and UV spectroscopies combined to position the energy levels of TiO2 anatase and rutile nanopowders, Phys. Chem. Chem. Phys. 20 (40) (2018) 25629–25637.
[41] J. Fu, X. Lu, P.E. Savage, Catalytic hydrothermal deoxygenation of palmitic acid, Energy Environ. Sci. 3 (3) (2010) 311–317.
[42] G.D. Yadav, P.K. Goel, Selective synthesis of perfumery grade cyclohexyl esters from cyclohexene and carboxylic acids over ion exchange resins: an example of 100% atom economy, Green Chem. 2 (2) (2000) 71–78.
[43] B. Oliver-Tomas, et al., Effect of the Cα substitution on the ketonic decarboxylation of carboxylic acids over m-ZrO2: the role of entropy, Catal. Sci. Technol. 6 (14) (2016) 5561–5566.
[44] A.V. Ignatchenko, E.I. Kozliak, Distinguishing enolic and carbonyl components in the mechanism of carboxylic acid ketonization on monoclinic zirconia, ACS Catal. 2 (8) (2012) 1555–1562.
[45] S. Shylesh, et al., Experimental and computational studies of carbon–carbon bond formation via ketonization and aldol condensation over site-isolated zirconium catalysts, ACS Catal. 10 (8) (2020) 4566–4579.
[46] H. Bayahia, E.F. Kozhevnikova, I.V. Kozhevnikov, Ketonisation of carboxylic acids over Zn-Cr oxide in the gas phase, Appl. Catal. B Environ. 165 (2015) 253–259.
[47] J. Kanervo, S. Toppinen, P. Nurmi, Method for Producing Ketones for Fuel and Oil Applications, NESTE OYJ: US, 2019.
[48] R.L. Stevenson, et al., Fluid Phase Equilibria and critical phenomena for the dodecane-water and squalane-water systems at elevated temperatures and pressures, Fluid Phase Equilibria 93 (1994) 317–336.
[49] H.M. Sebastian, et al., Vapor-liquid equilibrium in binary mixtures of carbon dioxide + n-decane and carbon dioxide + n-hexadecane, J. Chem. Eng. Data 25 (2) (1980) 138–140.
[50] M.A. Hasan, M.I. Zaki, L. Pasupulety, Oxide-catalyzed conversion of acetic acid into acetone: an FTIR spectroscopic investigation, Appl. Catal. A Gen. 243 (1) (2003) 81–92.
[51] U. Tumuluri, et al., Effect of surface structure of TiO2 nanoparticles on CO_2 adsorption and SO2 resistance, ACS Sustain. Chem. Eng. 5 (10) (2017) 9295–9306.
[52] A.V. Ignatchenko, A.J. Cohen, Reversibility of the catalytic ketonization of carboxylic acids and of beta-keto acids decarboxylation, Catal. Commun. 111 (2018) 104–107.
[53] A.V. Ignatchenko, et al., Equilibrium in the catalytic condensation of carboxylic acids with methyl ketones to 1,3-diketones and the origin of the reketonization effect, ACS Omega 4 (6) (2019) 11032–11043.
[54] C.A. Gaertner, et al., Ketonization reactions of carboxylic acids and esters over ceria−zirconia as biomass-upgrading processes, Ind. Eng. Chem. Res. 49 (13) (2010) 6027–6033.
[55] E.V. Fufachev, B.M. Weckhuysen, P.C.A. Bruijnincx, Crystal phase effects on the gas-phase ketonization of small carboxylic acids over TiO2 catalysts, ChemSusChem 14 (13) (2021) 2710–2720.